INVESTIGATING THE EFFECT OF DEFORMATION AND ANNEALING TEXTURE ON
MAGNETIC ANISOTROPY IN LOW-C STEEL SHEETS
BY
MAGNETIC BARKHAUSEN NOISE METHOD

A THESIS SUBMITTED TO
THE GRADUATE SCHOOL OF NATURAL AND APPLIED SCIENCES
OF
MIDDLE EAST TECHNICAL UNIVERSITY

BY

FEHMİ ÜMİT AKÇAOĞLU

IN PARTIAL FULFILLMENT OF THE REQUIREMENTS
FOR
THE DEGREE OF MASTER OF SCIENCE
IN
METALLURGICAL AND MATERIALS ENGINEERING

January 2013

Approval of the thesis:

**INVESTIGATING THE EFFECT OF DEFORMATION AND ANNEALING TEXTURE ON
MAGNETIC ANISOTROPY IN LOW-C STEEL SHEETS
BY
MAGNETIC BARKHAUSEN NOISE METHOD**

Submitted by **FEHMİ ÜMİT AKÇAOĞLU** in partial fulfillment of the requirements for the degree of **Master of Science in Metallurgical and Materials Engineering Department, Middle East Technical University** by

Prof Dr. Canan ÖZGEN
Dean, Graduate School of **Natural and Applied Sciences**   ——————

Prof. Dr. C. Hakan GÜR
Head of Department, **Metallurgical and Materials Engineering**   ——————

Prof. Dr. C. Hakan GÜR
Supervisor, **Metallurgical and Materials Engineering Dept., METU**   ——————

Examining Committee Members:

Prof. Dr. Tayfur ÖZTÜRK
Metallurgical and Materials Eng. Dept., METU   ——————

Prof. Dr. C. Hakan GÜR
Metallurgical and Materials Eng. Dept., METU   ——————

Prof. Dr. Rıza GÜRBÜZ
Metallurgical and Materials Eng. Dept., METU   ——————

Prof. Dr. Bülent DOYUM
Metallurgical and Materials Eng. Dept., METU   ——————

Dr. İbrahim ÇAM
Central Laboratory, METU   ——————

Date: 31.01.2013

I hereby declare that all information in this document has been obtained and presented in accordance with academic rules and ethical conduct. I also declare that, as required by these rules and conduct, I have fully cited and referenced all material and results that are not original to this work.

Name, Last name: Fehmi Ümit AKÇAOĞLU

Signature:

ABSTRACT

INVESTIGATING THE EFFECT OF DEFORMATION AND ANNEALING TEXTURE ON
MAGNETIC ANISOTROPY IN LOW-C STEEL SHEETS
BY
MAGNETIC BARKHAUSEN NOISE METHOD

AKÇAOĞLU, Fehmi Ümit
M.S., Department of Metallurgical and Materials Engineering
Supervisor: Prof. Dr. C. Hakan GÜR

January 2013, 55 Pages

Deformation and annealing texture in the cold rolled low carbon steels is important for sheet metal forming operations and service performance. The aim of this study is to non-destructively investigate the effect of texture on magnetic anisotropy. Various samples having different textures and residual stress states, due to different % reduction in thickness, annealing and stress relieving treatment, were prepared. Texture maps were obtained by Magnetic Barkhausen noise measurements performed with 10^0 steps between the ranges of 0^0-360^0 on the surface. Microstructure investigation by optical & scanning electron microscopy; hardness and tension tests were performed; and texture was determined by X-Ray diffraction method. The results were compared, evaluated and discussed to establish relationship between texture and magnetic Barkhausen Noise emission.

Keywords: Steel, Sheet Metal, Temper Rolling, Texture, Non-destructive Materials Characterization, Magnetic Barkhausen Noise

ÖZ

DÜŞÜK KARBONLU ÇELİK SACLARDA DEFORMASYON VE TAVLAMA DOKUSUNUN
MANYETİK ANİZOTROPİ ÜZERİNE ETKİSİNİN
MANYETİK BARKHAUSEN GÜRÜLTÜSÜ YÖNTEMİ İLE İNCELENMESİ

AKÇAOĞLU, Fehmi Ümit
Yüksek Lisans, Metalurji ve Malzeme Mühendisliği Bölümü
Tez Yöneticisi: Prof. Dr. C. Hakan GÜR

Ocak 2013, 55 Sayfa

Soğuk haddelenmiş ve tavlanmış düşük karbonlu çelik saçlarda doku oluşumu, takiben uygulanacak şekillendirme işlemleri ve servis performansı açısından önemlidir. Bu çalışmanın amacı, doku oluşumunun manyetik anizotropi üzerine olan etkisini tahribatsız olarak incelemektir. Farklı miktarlarda haddelemenin, tavlamanın ve gerilim gidermenin neden olduğu çeşitli doku ve kalıntı gerilim miktarlarına sahip olan numuneler hazırlanmıştır. 10° adımlarla $0-360^{0}$ aralığında Manyetik Barkhausen Gürültüsü ölçümleri yapılarak manyetik anizotropy haritaları çıkarılmıştır. Optik ve Taramalı Elektron Mikroskobu ile mikro yapı incelenmiş, sertlik ve çekme testleri uygulanmış ve X-ışını kırınımı metoduyla doku tayini yapılmıştır. Doku yapısı ile Barkhausen Gürültüsü sinyalleri arasında bağıntı kurulması amacıyla sonuçlar değerlendirilmiş ve karşılaştırılmıştır.

Anahtar Kelimeler: Çelik, Sac, Temper Haddesi, Doku, Tahribatsız Malzeme Karakterizasyonu, Manyetik Barkhausen Gürültüsü

To my family

ACKNOWLEDGEMENTS

TABLE OF CONTENTS

LIST OF TABLES

TABLES

LIST OF FIGURES

FIGURES

CHAPTER 1

INTRODUCTION

1.1 General

Low carbon steels are widely used due to their reproducing, processing, welding and high drawability capabilities despite their low production costs. These steels are very essential in automotive and aerospace industry for many years mainly for their high shape and thickness alternatives.

Low carbon steels have a lower mechanical property value when compared to medium and high carbon steels and they can also be alloyed as they are used in non-treated state. Hence, they are usually cold treated to enhance their mechanical properties and for higher homogeneity through the whole part and accuracy in thickness. As a result of severe uniaxial plastic deformation, a preferred orientation, texture forms. Concordantly, certain crystallographic planes tend to orient themselves in a preferred manner with respect to the direction of maximum strain which leads to anisotropy in mechanical properties.

Quality control of the cold deformed steels including texture is vital. Traditional ways of quality control on a production line contains cutting a representative sample following the preparation stages. Since traditional methods (r and Δr calculation, X-Ray diffraction, EBSD) are destructive, time consuming and a hundred percent inspection is impossible, there is an interest to develop nondestructive techniques capable of rapid evaluation. Thus, development of nondestructive techniques for minimizing the production time and characterization of microstructure has been a challenging task in recent decades.

1.2 Deformation Induced Texture

When metals were hot deformed, i.e. above the recrystallization temperature, the work hardening produced by deformation tends to be counteracted by recovery process. Recovery causes rearrangement and annihilation of dislocations so that, as strain increases, the dislocations tend to form into two dimensional subgrain walls. In some metals and alloys the recovery entirely balances work hardening, and steady state is achieved and can be maintained to large strains before fracture occurs [1].

Cold working, deforming below recrystallization temperature, strengthens a metal through work hardening or strain hardening. When the mechanical stress on a metal becomes high enough, it causes permanent crystallographic defects called dislocations in the crystalline structure. As the number of dislocations increases, it becomes more difficult for new dislocations to form or for existing defects to move through the crystal structure, making the metal becomes more resistant to further deformation [2].

A metal which has undergone a severe amount of uniaxial plastic deformation (Figure 1-1), as in rolling or wire drawing, will develop a preferred orientation or *texture* in which certain

crystallographic planes tend to orient themselves in a preferred manner with respect to the direction of maximum strain.
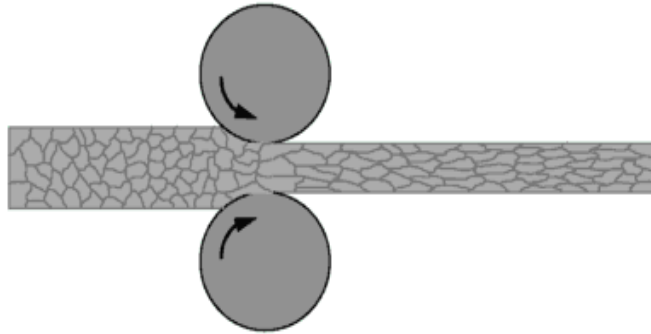
Figure 1-1 Schematic representation of rolling process and grain elongation

The formation of texture is an extremely important phenomenon from a commercial point of view because it results in highly anisotropic physical properties in sheet materials. In order to improve the performance and service life of steel components optimization and control of texture and the anisotropic properties is very important in industrial production.

There are several ways to determine the texture formation in a metal during cold deformation. If measurement is made by the radiation sources, the texture analysis is made in two scales which are micro-texture techniques (based usually on electron diffraction) and macro-texture techniques (based on x-ray or neutron diffraction). For macro-texture techniques, the primary output is a profile of diffracted intensities, which is characteristic of a large contiguous sample volume. By the X-Ray technique a texture is often described with a pole figure on a micrographic projection. For microtexture (individual grain) techniques, the primary output is a diffraction pattern from each sampled volume [3].

Lankfort coefficients (r & Δr values), given in Equations 1.1 to 1.4, are determined in order to explain the anisotropic behavior of cold rolled metals. These are a measure of the plastic anisotropy. And used as an indicator of the formability of low carbon sheet steels.

$$r = \frac{\ln \dfrac{w}{w_0}}{\ln \dfrac{t}{t_0}} \tag{1.1}$$

Where w_0 and w are the initial and final widths, while t_0 and t are the initial and final thicknesses of the specimen [4]. For a good drawability, steel requires high r-value (>1) in order to minimize the local reduction of the thickness during the forming operation.

The average of the r-values obtained for different directions in the plane of the sheet metal represents the so-called coefficient of normal anisotropy r_n. Having determined the values of r at specimens cut along three directions in the plane of the sheet metal (0^0, 45^0, 90^0, respectively, Figure 1-4), the coefficient of normal anisotropy is determined by:

$$\bar{r} = \frac{r_0 + 2r_{45} + r_{90}}{4} \tag{1.2}$$

2

However, r-value is generally not constant over the various directions within the steel sheets. Planar anisotropy, a measure of the variation of normal anisotropy with the angle to the rolling direction, is as given in Eq^n 1.3.

$$\Delta r = \frac{r_0 + r_{90} - 2r_{45}}{2}$$
(1.3)

A low planar anisotropy ($\Delta r \approx 0$) combining with high mean r-value, r_m, leads an optimal deep drawing performance where mean r-value defined in Eq^n 1.4.

$$r_m = \frac{r_0 + 2r_{45} + r_{90}}{4}$$
(1.4)

Figure 1-2 shows the effect of carbon content and Figure 1-3 shows the effect of cold reduction on r_m value.
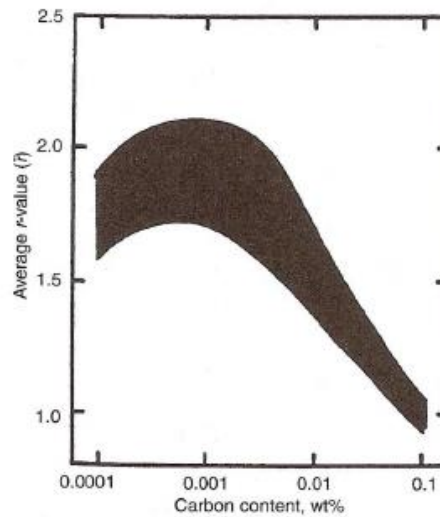
Figure 1-2 r_m variation with increasing steel carbon content [5]
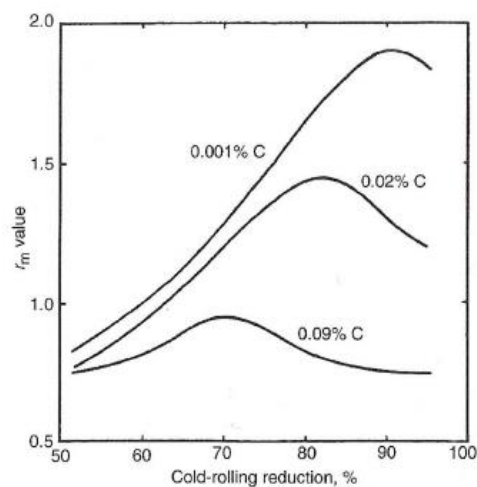
Figure 1-3 Effect of cold reduction on r_m values with different carbon content [6]

3
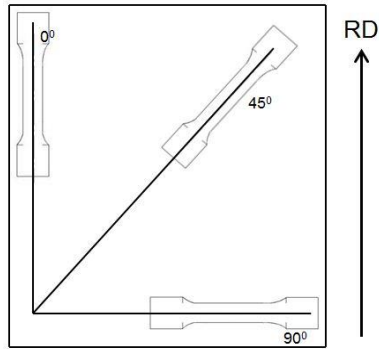
Figure 1-4 Preparation of the tensile test specimens

Another method to measure anisotropic effect of texture formation is ultrasonic measurement. Measurement technique uses the angular variation of the ultrasonic waves in the sheet to detect texture and directionality. The effect of texture on velocity of an ultrasonic wave is to slow it down in one direction and make it faster in another (Figure 1-5). Ultrasonic velocity measurements take advantage of this effect, thus determining the formability and texture parameters such as the r.
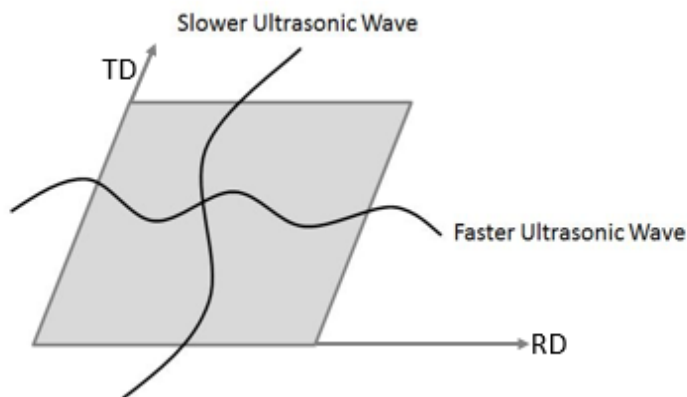
Figure 1-5 Directional dependence of sound velocity in a cold rolled sheet

Various experimental and numerical studies had shown that residual stress on the surface of a cold rolled sheet is in compressive state [7, 8]. The reason is that the strain difference between the surface and the internal of the sheet formed during the rolling process (Figure 1-6).
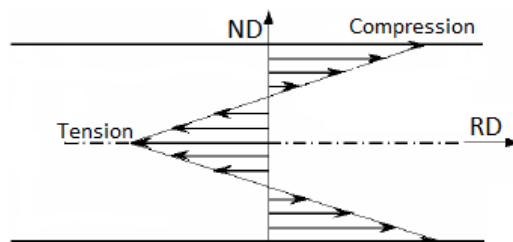
Figure 1-6 Residual stress distribution in the cross section of cold rolled sheet [7, 8]

4

The simplest deformation texture is produced by the rolling which is often referred to as a *fiber texture* because of its similarity with the arrangement in naturally fibrous materials.

There are three basic planes for a rolled steel to explain the texture direction which are rolling direction (RD), transverse direction (TD) and normal direction (ND) as shown in Figure 1-7.
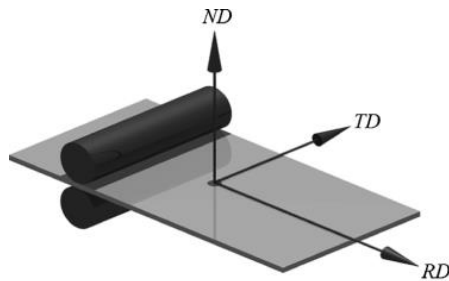
Figure 1-7 Representation of the directions on a rolled sheet

The deformation texture of a sheet produced by rolling is described by the crystallographic planes as well as the crystallographic directions in that plane which are parallel to these directions.

In a cold rolled sheet, texture components vary with the reduction ratios. A preferred orientation of the grains is evident in BCC metals at reduction ratios exceeding 40%. A weak component of {001} <100> formation was observed in cold reduction ratios up to 60%, but increasing cold deformation produced strong <110> fiber texture with {001} <110> and {112} <110> maximum peak position in rolling direction which is also called as α fiber [9, 10].

In γ fibering, i.e. texture formation parallel to the normal direction starts with a weak component of {110} <001>. Increasing reduction ratios leads stronger texture components of {111} <112> and {111} <110>. Both of the fiber formations end up with the same orientation which is {223} <110>.

1.3 Recrystallization Texture in Cold Rolled Low Carbon Sheet Steels

Both nucleation and growth mechanisms determine the recrystallization texture. Since the stored energy determines which of the nucleation mechanism for recrystallization will dominate, annealing texture is dependent on it. The SIBM (Stress Induced Grain Boundary Migration) nucleation mechanism dominates in the case of low stored energy which allows low energy {001} <100> or {112} <110> subgrains to grow into high energy areas. On the other hand, if the grains have high stored energy, nucleation may occur by the subgrain growth mechanism which generally favors the formation of {111} <100> and {110} <110> components [11].

Initial grain size is another factor that affect the recrystallization texture where initial grain size increases the γ fibre intensity. Also, *r*-value shows an increase with decreasing initial grain size.

The variation in fraction of texture components for the low carbon steels with annealing time is given in Figure 1-8 [12]. The volume fraction of α and γ texture components does not change up to the mid stage of recrystallization, thereafter the {111} <112> component starts to increase while the {112} <110> component starts to decrease. The intensity of the {111} <110> component is remained in same values and slightly increases at the end of recrystallization process. {001} <110> components maintain for a long time and decreases rapidly at the late stage of recrystallization.
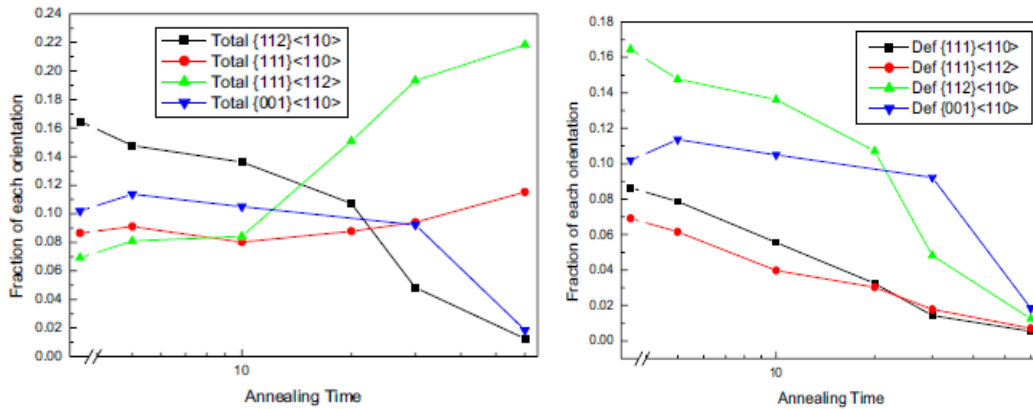
Figure 1-8 Volume fractions of texture components with annealing time [12]

1.4 Magnetic Barkhausen Noise Method

MBN (Magnetic Barkhausen Noise) is a non-destructive technique using the magnetic domain walls (Bloch walls) movement by the application of magnetic field into a ferromagnetic material. Generally, in a MBN set up a gauge counts the noise made by the magnetic domain walls movement over the pinning sites of a polycrsytal specimen. A detailed definition is necessary for the causes of these noises.

A natural polycrystalline ferromagnetic material consists of many magnetic domains which are randomly oriented (Figure 1-9). As a result the total magnetization of the material is equal to zero. But, when an electric field is applied to the sample these domains align themselves with the direction of the applied field and the sample gets magnetized. [13]
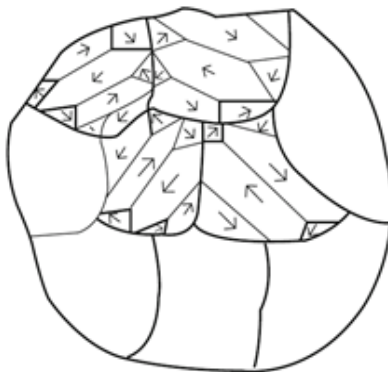
Figure 1-9 Magnetic domains in a ferromagnetic material with zero magnetization [13]

During the magnetization process, domains with the same direction with magnetization get bigger in size and the remaining ones get smaller. This phenomenon occurs by the domain wall motion (Figure 1-10) and rotation of domains.
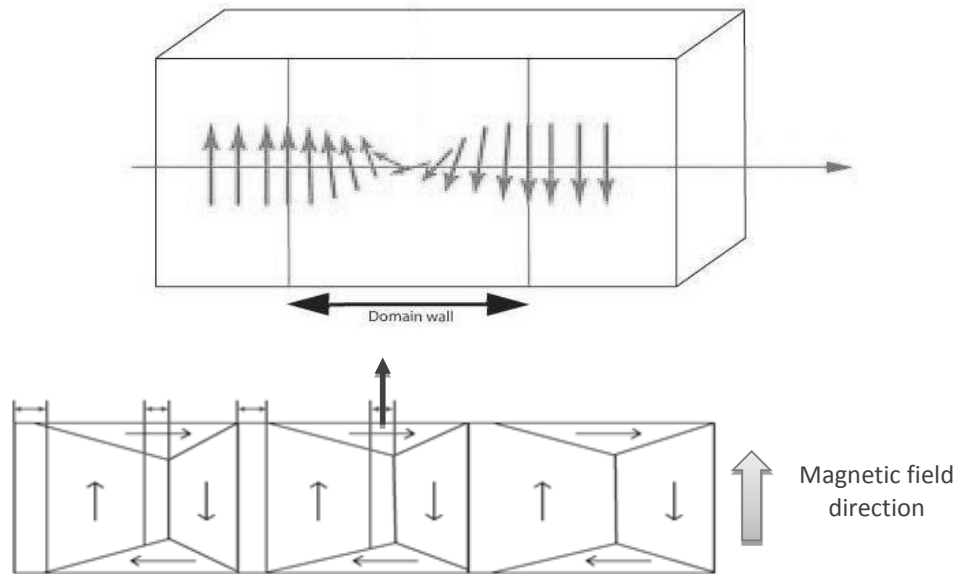
Figure 1-10 Domain wall displacement under the influence of a magnetic field

Magnetization and demagnetization in ferromagnetic materials are irreversible processes called as magnetic hysteresis. This phenomenon is crucial to explore the physics behind ferromagnetic magnetism. Three parameters which can be obtained from the hysteresis curve are magnetic induction (B), applied magnetic field strength (H) and permeability (μ) [14]. Permeability is the degree of magnetization of a material in response to a magnetic field and the relation between these three parameters are:

$$B = \mu.H \tag{1.5}$$

The alteration of domain structure in a ferromagnetic material consists of two different stages. Applied magnetic field which has low intensity, cause a reversible change in the domain walls. This kind of a change can be reverted to a non-magnetized state after magnetic field disappears. However, a higher amounted magnetic field let imperfections which exist in crystalline structure (pinning sites) to move past and after that, this phenomenon becomes irreversible and finally this event continues until the magnetic structure gets a single domain. When the actions of domain wall motion completed, higher amounted magnetic field causes a domain rotation and produces a relatively small increase in magnetization which depends on magnetocrystalline energy of the material (Figure 1-11).
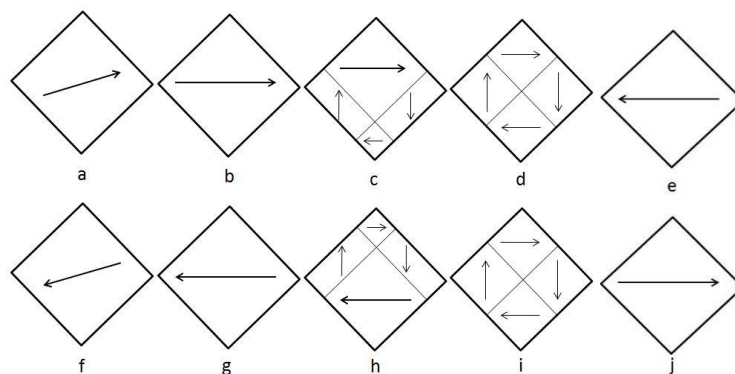
Figure 1-11 Domain structure during magnetization

This reached limit is called as the *saturation* point which means the material cannot be magnetized anymore. In case of a removal of the magnetization field, domains can never reverse back to their original positions. This magnetization is called as *remanent* magnetization (*retentivity*) which is described by the formula of,

$$B_R = \mu_o.M_R \tag{1.6}$$

where μ_o is vacuum permeability, B_R is remanent induction and M_R is remanent magnetization.

Coercive field (*coercivity*) is the field required to reduce the magnetization of the sample to zero (Figure 1-12). The entire phenomenon is explained below and the magnetic domains structures during these processes are schematically represented in Figure 1-12.
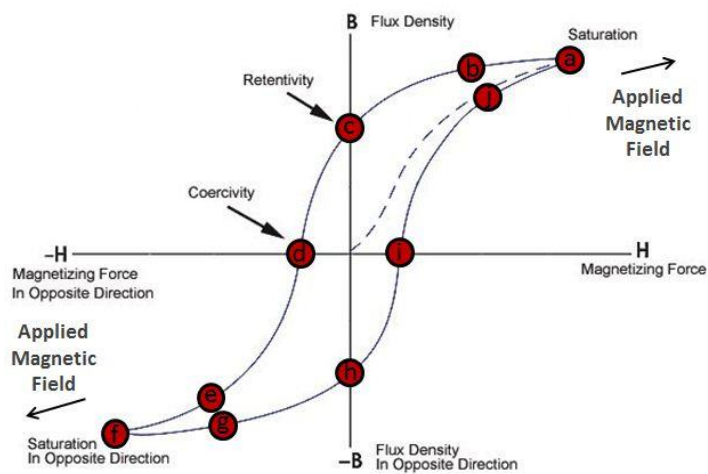
Figure 1-12 Hysteresis curve of a ferromagnetic material

This alignment has a certain ratio for every material but basically magnetization of the sample changes as shown in the Figure 1-13.
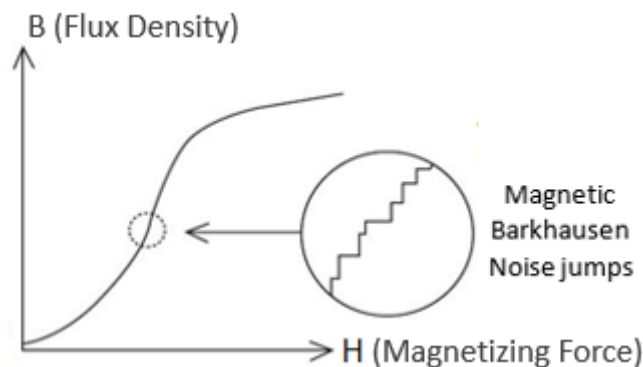
Figure 1-13 Irreversible discontinuities during the magnetization of a ferromagnetic material [2]

The motion of the domain walls are not solid, i.e. each energy level yields the wall to exceed a barrier and continue its path. The reason is the pinning sites contained in the crystal structure of the material like grain boundaries, dislocations, inhomogeneity's or other imperfections. All lattice irregularities are like to cause delays in domain wall movement, leading to uneven and discontinuous changes in magnetization [15].

These abrupt changes were firstly discovered in 1919 by H. Barkhausen [16] with a wire wounded ferromagnetic specimen which hooked to an external speaker. He found that the verification of magnetic field around the specimen caused a rushing sound in speaker. This rushing sound was occurred as a result of small changes in magnetic flux within the confines of the coil which are called as *Barkhausen Noise*.

With the intention of Barkhausen perform measurement, two different techniques are applicable [17]. While in one of these techniques, Barkhausen noise is obtained by siting the detection coil above the sample, in the other technique, it is obtained by wrapping around the sample and named as encircling Barkhausen noise (Figure 1-14).
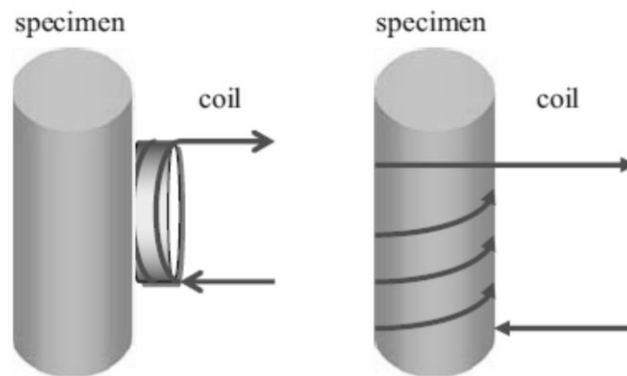
Figure 1-14 Surface and encircling Barkhausen noise techniques [13]

A typical set up of a Barkhausen Test equipment is shown in Figure 1-15.
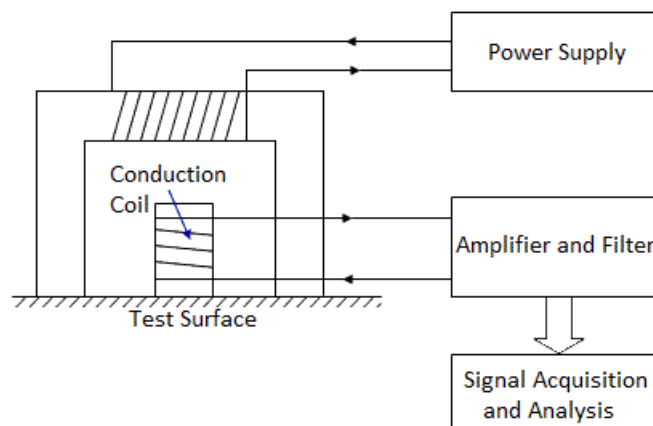
Figure 1-15 A typical MBN system set up [18]

Depth of Magnetic Barkhausen Noise measurement can be calculated by Eq^n 1.7.

$$\delta = \frac{1}{\sqrt{\pi.f.\sigma.\mu_r.\mu_o}}$$

(1.7)

where

σ : Conductivity ($\Omega^{-1}m^{-1}$)

f : Frequency content of MBN (Hz)

μ_r : Relative permeability

μ_o : Permeability of vacuum (N.A^{-2})

Study made by Moorthy et al. [19] shows skin depth of 150 to 20 μm for 20 to 1000 kHz frequency ranges. Since low carbon steel has higher relative permeability (6000), for the same frequency range maximum 10 μm of skin depth can be obtained.

There are certain transition layers between the domains which show different magnetism orientation. These transition regions are called as Bloch Walls and classified by the angle of magnetization direction of domains. Domain walls separating regions of opposite magnetic moment are called 180^0 walls, whereas walls lying at 90^0 to each other are appropriately termed 90^0 walls (Figure 1-16) [20, 21]. It is believed that MBN is primarily due to 180^0 domain wall motion because of their larger average velocity and larger sweep area than 90^0 walls.
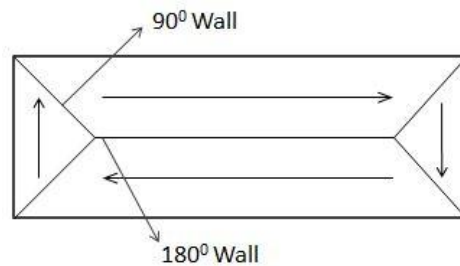
Figure 1-16 Schematic representation of 90^0 and 180^0 domain walls

In another study made on the grain oriented 3% Si-Fe material, it is pointed out that domain wall energy for 90^0 (0.62 ergs/cc) is lower than 180^0 domain wall energy (1.24 ergs/cc) for [100] direction.

Before the explanation of the wall movement through the pinning sites it is necessary to have enough knowledge about the formation of magnetic domains. Ferromagnetic materials are composed of domains because of energy minimization requirements. The total energy is the summation of five basic energies [13, 17, 22, 21, 23].

$$E_{total} = E_{exchange} + E_{magnetostatic} + E_{magnetocrystalline} + E_{magnetoelastic} + E_{wall}$$

(1.8)

E_exchange: It originates in quantum mechanical exchange forces or spin–spin interactions that are responsible for ferromagnetism.

E_magnetostatic: It reaches a minimum when the magnetization of a magnetic domain is parallel to the external magnetic field.

E_{magnetocrystalline}: Crystal symmetry gives rise to a magnetocrystalline (anisotropic) energy that becomes minimum when the magnetization of a magnetic domain is aligned with a preferred crystallographic direction, such as <100> in α iron which is called magnetic easy axis. Also, <110> is called as magnetic medium and <111> is called as magnetic hard axis (Figure 1-17).
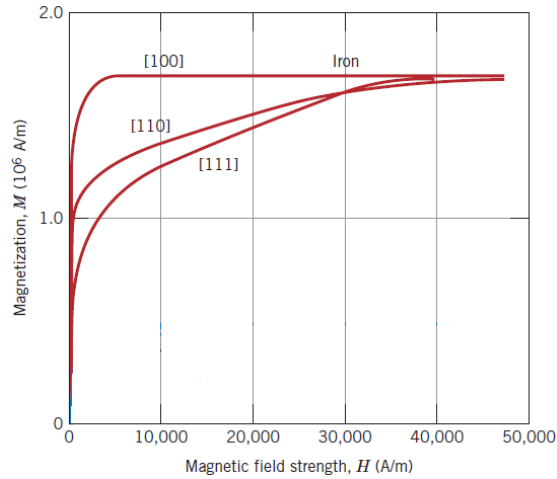
Figure 1-17 Magnetization curves for single crystals of iron [24]

E_{magnetoalestic}: The crystal lattice strain is related to the direction of domain magnetization through the magnetoelastic energy. It is a minimum when the lattice is deformed such that the domain is elongated or contracted in the direction of domain magnetization.

E_{wall} (90⁰ & 180⁰): It is related to the fact that domain walls have certain energy per unit area of surface and unit thickness.

Increases or decreases may occur in any of these energy states in order to maintain the minimum total energy and these changes can be evaluated for non-destructive evaluation of magnetic materials.

The raw MBN data (Figure 1-18) gives voltage distribution as a function of time which is associated with applied magnetic field. By the filtering of this data following parameters can be obtained:

MBN fingerprint: It shows maximum noise amplitude (peak height) and the corresponding magnetic field (peak position). Applied magnetic field is plotted against a calculated local root-mean-square (RMS) value and a smoothing algorithm might be applied to obtain MBN fingerprint (Figure 1-19-a).

Frequency spectrum: Fast Fourier Transform is applied to convert time into frequency in order to determine the spectral content of time domain signals which is given by square of voltage (V^2). (Figure 1-19-b)

Pulse height distribution: It gives the number of pulses (events) against the pulse amplitude and variation is depend on the pinning sites within the material. (Figure 1-19-c)

B-H (Hysteresis) curve: It corresponds to a curve which gives coercivity, remanence and permeability values of the materials. But, local MBN measurement gives a representative value which can not be used as a true one. (Figure 1-19-d)
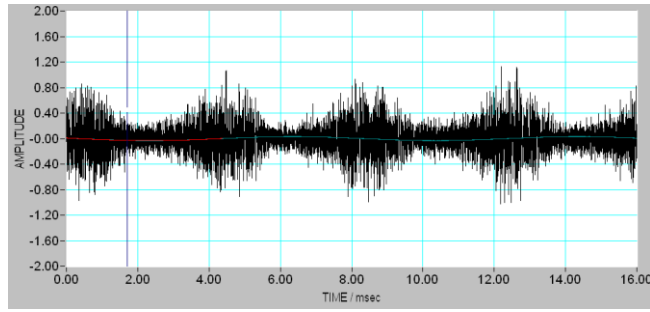
Figure 1-18 Raw MBN data

| a | b |
| c | d |
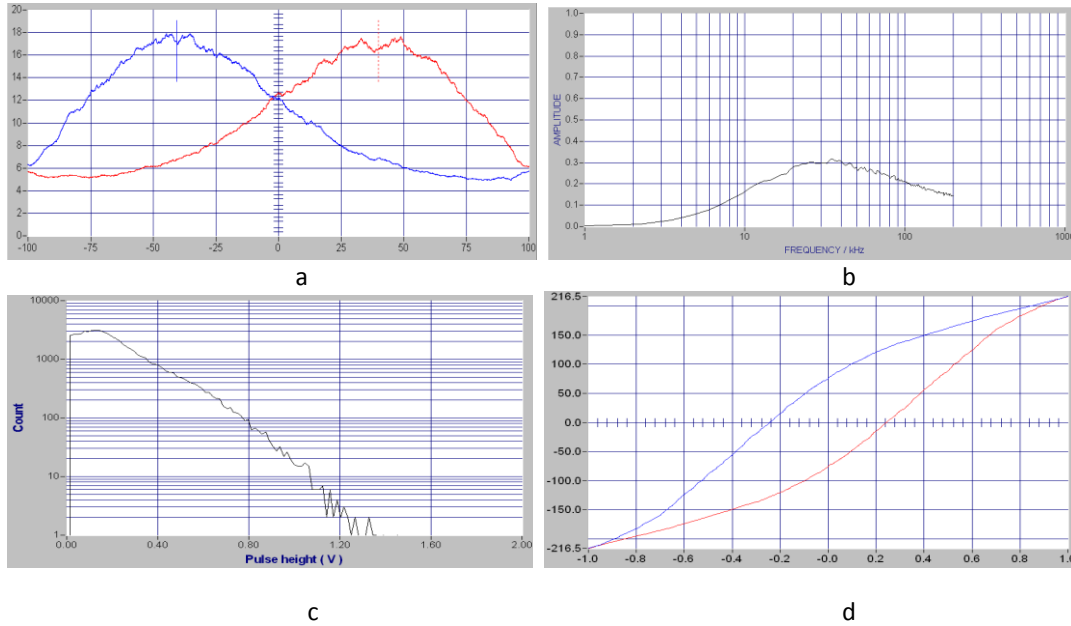
Figure 1-19 (a) MBN fingerprint, (b) frequency spectrum, (c) pulse height distribution, (d) B-H curve

1.4.1 Magnetic Anisotropy

The phenomenon of direction dependence of a magnetic material is called magnetic anisotropy. A metal which behaves as magnetically isotropic has materially no preferential direction, in the absence of a magnetic field. However, according to measurements made in a magnetically anisotropic material indicates that the sample constitutes an easy axis in itself.

Magnetic anisotropy can be effectively characterized by "angular dependent" Barkhausen noise technique. MBN signals are detected at particular angles with respect to the specimen's axis and measured values are plotted on a polar graph. Thanks to the emerging shape of polar graph, looking at the amount of Barkhausen noise, it is possible to comment not only about the direction of magnetic easy axis but also about anisotropy of the material. This method has been used to determine the magnetic easy axis in 3% Si-Fe laminates [25] and pipeline steels [26].

A typical magnetic easy axis representation is shown in Figure 1-20. MBN $_{energy}$ term is used to characterize the MBN measurement at a given sample location.

$$MBN_{energy} = \alpha \cos^2(\theta - \phi) + \beta \qquad (1.9)$$

where α is associated with the angular-dependent variation of the MBN signal, and it is related to the $180°$ domain wall motion associated with domains that define the magnetic easy axis direction

[27, 28]. β parameter is the angular-independent portion of the MBN signal, and φ is the direction of magnetic easy axis with respect to the fixed reference system.

The proportion of the anisotropy in magnetic properties can be calculated by using MBN energy ratio (Figure 1-21) given in Eq^n 1.10.

$$MBN_{energy\ ratio} = \frac{MBN_{energy}(\theta = 0^0)}{MBN_{energy}(\theta = 90^0)}$$

(1.10)

where the angle θ is measured with respect to the axial magnetizing direction.
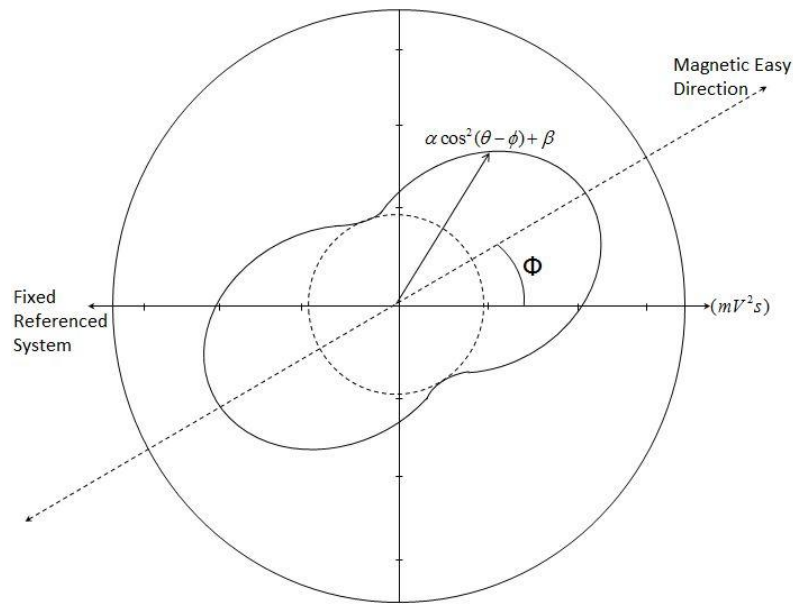
Figure 1-20 Parameters used to define the MBN energy [27]
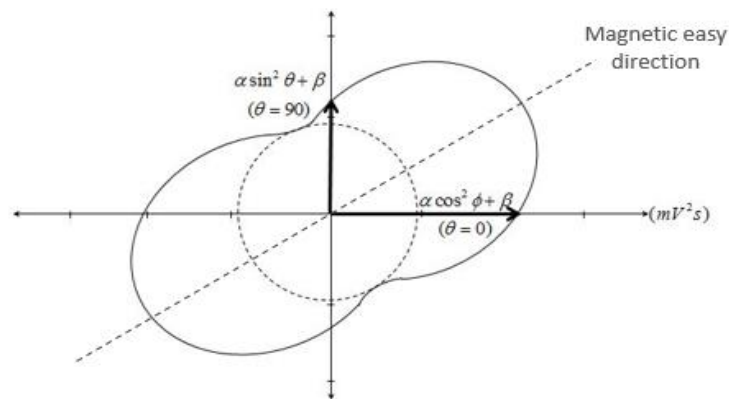
Figure 1-21 Graphical representation of MBN energy ratio [27]

Magnetic anisotropy of cold rolled low C steels which have reduction ratios varying between 0% and 60% was studied by Stefanita et al. and angular change in Magnetic Barkhausen Noise is studied. α

and β parameters are shown in the outcomes, additionally, effects of crystallographic texture macroscopic residual stresses, and microstructure are examined through alterations in magnetic easy direction [29]. An initial magnetic easy direction, resulting from crystallographic texture, parallel to the rolling direction is destroyed with cold deformation and replaced with transverse magnetic easy direction. It is assumed that the reason for this shift is macroscopic axial compressive stresses developed at the sample surface during rolling.

The main factors having important role in the formation of Barkhausen Noise can be classified under three headings: microstructure (average grain size, phases, etc.), stress (residual stress, external elastic stresses), and crystal structure.

1.4.2 Effect of Microstructure on Barkhausen Noise

Formation of the Barkhausen noise is comprised of a pinning site effect, and as a result of this formation, it is expected that the effect of grain boundary to the amount of emission should be relatively high. Samples annealed at lower temperatures have larger number of grain boundaries with smaller grains than samples annealed at high temperatures. Since the grain boundaries act as pinning sites small grain samples emits larger MBN signals, and more pinning sites need to be overcome when the walls move, because of their large fractional volume.

According to studies conducted on pure iron samples [30] the RMS values decreased as grain size increased from 50 μm to 180 μm which satisfies a Petch-like relationship. Also, it was reported that MBN peak height decreased as ferrite grains get coarser from 50 to 300 μm for ultrahigh purity iron [31].

The relation between RMS (root mean square) of MBN signals and AGS (average grain size) is given in Eq^n 1.11 [32, 33]:

$$RMS = k.(AGS)^{-0.5}$$
(1.11)

"k" is a parameter independent of grain size, but depends on magnetic field strength, quantity of magnetic flux change, wall energy per unit area, etc. [14] Recent search also shows that the coarser grain structure results with the lower MBN activity.

Another microstructural factors effecting the formation of Barkhausen Noise is dislocation density. Increased plastic deformation generates different dislocation structures. In lower strain values, isolated dislocations at first exist in grain boundary regions, later on move forward to grain interiors. In the higher strain ratios, on the other hand, because of increased density of dislocations, dislocation tangles become integrated and these tangles of dislocations become interconnected which forms rough cellular structure consisting of high dislocation density walls separated by low dislocation density regions.

According to the results of a study conducted on high purity iron [34], Barkhausen emission increases with the increase of dislocation density; however, increasing values of dislocation tangles, as a result of higher strain values, prevent the formation of the Barkhausen noise and decreases the emission.

Microstructure effect on Barkhausen Noise emission in the cold-rolled low C steel has been reported by Bükki-Deme et al. Barkhausen noise depth profile of steel sheets performed and also emission changes has been proved between rolling direction and transverse direction. [35]

Study made by Sagar et al. showed that cold rolled stainless steels which had different volume of martensitic phase and different reduction in thickness values (0, 10, 30, 50, 70, 90%) had magnetic easy axis parallel to the rolling direction due to relationship between austenitic and ferritic phases. X-Ray diffraction measurements showed <110> orientation with magnetic easy axis formation and also estimation between <100> texture formation and magnetization established with increasing cold reduction ratios [36].

Impacts of the changes in the chemical composition on the magnetic properties were researched. Jiles et al. [37] has reported the effect of varying carbon content of plain carbon steels on the magnetic properties and it shows that magnetic properties like coercivity and permeability have verifications as a function of carbon content. Every 0.1 wt% carbon addition increases the coercivity by 0.2 Oe while 0.2 wt% carbon addition decreases permeability by 57%. Also it has been found that the spheroidized samples were magnetically softer than the lamellar ones and the difference increased with the amount of the carbon content.

Influence of steel phases on Barkhausen noise have also been investigated [38] and the results are shown in Figure 1-22,
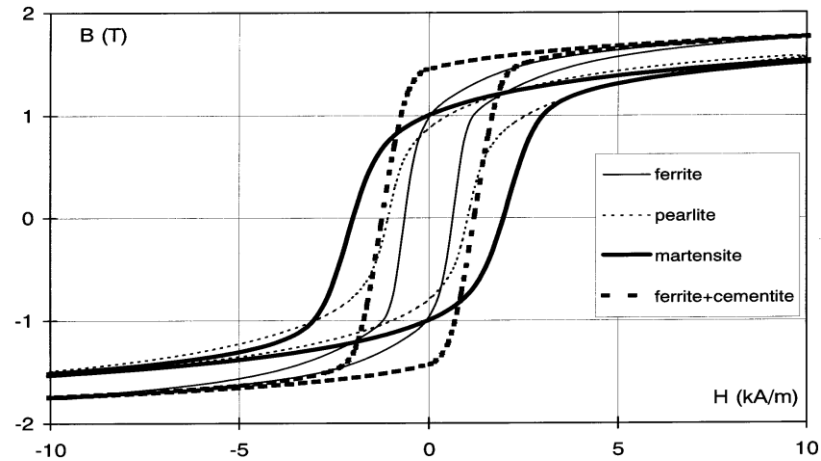
Figure 1-22 Hysteresis loops for different ferrite phases [38]

Various researches [39, 40] reported that, as the volume fraction of martensite increases, the peak voltage decreases which shows inverse proportion between martensite content and MBN activity.

Kameda et al. [41] reported that variations in MBN emissions are caused by the phase changes such as carbide precipitation or intergranular impurity segregation after heat treatment.

1.4.3 Effect of Stress on Barkhausen Noise

Application of an external stress, just like the effect of a magnetic field, overbalances the five types of energies. As a result, to be able to minimize the total value, domain movements become a part of the activity. In order to achieve this, domain realignment occurs with the movements of domain walls and a new configuration comes into existence. A new energy configuration is achieved when domains lying closest to the direction of applied uniaxial tensile stress grow at the expense of domains with perpendicular domain magnetization [13]. This phenomenon involves a reorientation of 180^0 domains into the <100> direction which is closest the stress direction. This is a result of strain energy (E_σ) contributed to a domain by stress (σ) applied at an angle (Θ) to the domain magnetization vector [39].

$$E_\sigma = \frac{3}{4}\lambda_{100}\sigma Tb\left[a+\left(a-\frac{b}{n}\right)\cos 2\Theta\right]$$

(1.12)

For a crystal of height a, b width, thickness T, and having n number of 180^0 domain walls. λ_{100} is the magnetostrictive saturation strain along <100> type directions. It is apparent that when Θ is 0 the energy is minimized which means 180^0 walls reorient themselves to align with the stress direction.

There is another mechanism through which magnetic domains respond to an applied stress. In general under stress, there is an increase in the 180^0 domain wall population in the stress direction if the stress is tensile, with an opposite effect for compressive stress. The energy change associated with adding an extra domain wall is determined by

$$\Delta E = -\frac{3}{4}\lambda_{100}\sigma b^2 T \frac{\cos 2\Theta}{n(n+1)} + \gamma_{180}aT + 3\delta\lambda_{100}\sigma aT \cos^2\Theta$$

(1.13)

where γ_{180} is the energy/area of the 180^0 domain walls and δ is the thickness of the 180^0 domain walls. Equation 1.13 indicates that the energy required to add a new domain increases for each time.

In addition to applied elastic and plastic strains, it is a known fact that residual stresses achieve the same effect to domain structures thereby to Barkhausen emission. While tensile residual stresses increases the Barkhausen intensity, compressive residual stresses reduces the Barkhausen noise level (Figure 1-23).
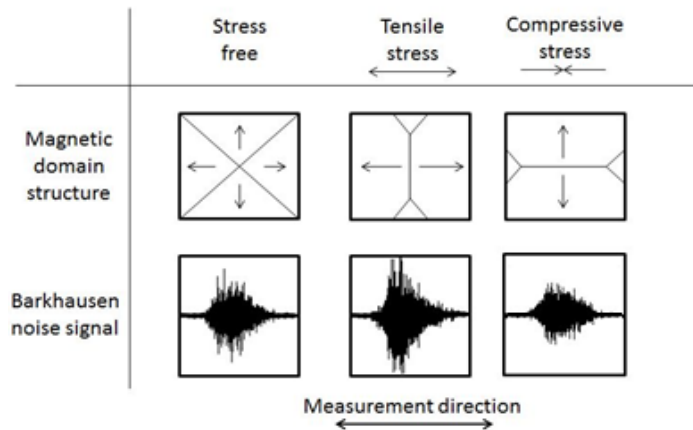
Figure 1-23 Barkhausen noise change due to stress [42]

Directionality of MBN emission of hot-rolled mild steel under tensile loading up to 20% straining was studied by Dhar et al. Anisotropy characterization were performed by calculating α and β parameters. Magnetic easy axis was observed in RD because of the increase in 180^0 wall intensity. Moreover, initially MBN energy increased but with increasing plastic deformation, it reached a saturation point in a decreasing manner [43]. In a similar work, [44] applied elastic and plastic deformations on a hot rolled mild steel with no initial crystallographic texture, causes an anisotropic energy increase in RD. Beside, average MBN energy was observed to increase in the early stages, however later stages it diminished.

Another directionality dependence of metals magnetic properties is examined by Campos and Sanches. They used ANSI 1050 steel which cold rolled in different reduction ratios and firstly angular variation measured with no tensile stress. Results show that MBN energy values and anisotropy characteristic changes with increasing reduction ratios due to formation of Lüder bands. For the second step MBN energy variation has been examined with the application of tensile stress parallel to the rolling direction and increase in the overall Barkhausen with the alteration of k (anisotropy)

parameter signal has been observed. Also other magnetism parameters (relative permeability and Hysteresis losses) have been established. [45]

1.4.4 Effect of Crystal Structure on Barkhausen Noise

A polycrystalline material which is not influenced by any stress or magnetic field may act as isotropic. However, as a result of magnetocrystalline effect in an individual bcc iron grain magnetic vectors tend to align themselves along <100> direction, i.e. easy magnetization [21].

During cold deformation, like cold rolling, crystal orientations occur because of grain rotations. As a result of these deformations, crystallographic texture exists and it has a great impact on the creation of a bulk magnetic easy axis in a polycrystalline material [2].

Angular profile of magnetic properties in ASTM 36 steels has been studied while exposed to the uniaxial elastic and plastic tensile deformation [46]. Directional change in magnetic easy axis were explained through texture and stress state under the parameter of k ($MBN_{energy}0^o/MBN_{energy}90^o$) which shows the anisotropy in magnetic state has been evaluated.

In the study conducted by Vengrinovich and Tsurman, angular changes in Barkhausen noise were examined in high strength low alloy steels and bending forces. Barkhausen Directional Diagrams (DD) were created in tension areas. According to the anisotropy in magnetic property that had been extracted through Directional Diagrams, an atlas was designed which explains possible texture and stress states in a metal. Propounded DD types and their explanations are given in Figure 1-24 [47].
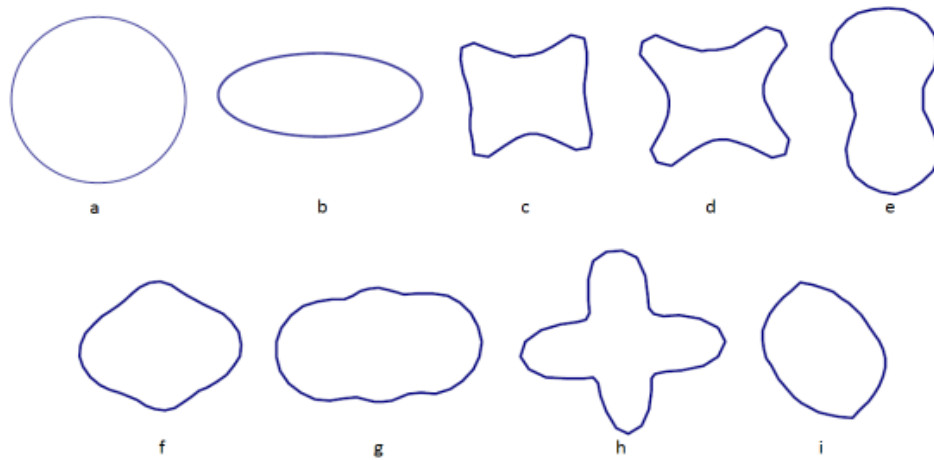
Figure 1-24 Typical examples of directional diagrams shapes for magnetic materials in various conditions: a) isotropic state; b) uni-axial tension or compression; c) bi-axial compression by two non-equal orthogonal loads; d) bi-axial compression by two equal orthogonal loads; e) large uni-axial bending; f) bi-axial tension by two non-equal orthogonal loads; g) small uni-axial bending; h) bi-axial tension by two equal orthogonal loads; i) weakly textured specimen with small applied tension [47].

1.5 Aim of the Study

Magnetic Barkhausen Noise method can carry out the information about ferromagnetic material's microstructural, mechanical and crystallographic properties. Since its advantages about being non-destructive, fastness and applicability to whole body, MBN method might be a good alternative to traditional methods.

In literature there is not any direct relation between texture and magnetic anisotropy in cold deformed or heat treated steel sheets. One of the main contributions of this study is characterizing the anisotropy in magnetic behavior and making a connection with the magnetic easy (100) and the medium (110) axis's in temper rolled steel sheets by Magnetic Barkhausen Noise method. The experimental studies cover metallographic examination, tension tests, hardness measurement, X-Ray texture measurement, and Magnetic Barkhausen Noise measurements. At the end, all experimental results were correlated.

CHAPTER 2

EXPERIMENTAL PROCEDURE

2.1 Material and Sample Preparation

In this study, a low carbon steel, produced by *temper rolling* (skin pass rolling) process was used, whose chemical composition is given in Table 2-1.

Table 2-1 Chemical composition of the samples (balance Fe)

	C	Si	Mn	P	S	Cr	Mo	Ni	Al	Co	Cu
%	0.02	0.003	0.14	0.01	0.004	0.02	0.004	0.015	0.04	0.004	0.025

Temper rolling process involves cold rolling of initial sheet metal with very slight reduction in which the degree of deformation is less than 2% where production of initial sheet metal has a number of processing steps including melting, casting, hot rolling, cold rolling and final annealing. The reason for the temper rolling is normally not perform in order to reduce the thickness of the strip, but to finalize the mechanical properties, planarity, and surface micro-relief of sheet metal and it prepares the sheet for its subsequent processing.

Since the impact of cold deformation on magnetic features is studied, analyses were performed on six different samples which have the same chemical composition but different % reduction in thicknesses. Dimensional and mechanical properties of the samples used in this study are presented in Table 2-2.

Table 2-2 The samples used

No	Initial Thickness (mm)	Final Thickness (mm)	% Reduction in Thickness (% RT)	r-value
1		1.15	48	1.27
2		0.97	56	1.66
3	2.2	0.80	64	1.68
4		0.60	73	1.66
5		0.50	77	2.15
6		0.40	82	1.73

2.2 Heat Treatments

Residual stresses and subcell structure generated due to cold deformation which affects MBN emission. To characterize these effects, second sample series were prepared by applying the stress relief heat treatment (500^0C/1 h) to the temper rolled samples.

In addition, a specific sample (no. 7) was prepared by normalizing (850^0C/1 hr; air cooling) of the sample no. 1 in order to remove all process effects completely.

2.3 Metallographic Investigations, Hardness and Tension Tests

For determining average grain size by intercept procedure according to ASTM E 112, and microstructures of the samples (Figure 2-1), optical microscopy and scanning electron microscopy (SEM) examinations were performed after mounting in bakelite, grinding, polishing and etching in %2 nital solution.

Figure 2-1 A representative sample for microstructural investigation.

Micro hardness measurements (HV 0.5) were done by Shimadzu hardness tester. 4.903 N (0.5 kg) load was applied for 10 seconds. For every sample at least 10 measurements were performed.

Three tensile test specimens were prepared (Figure 1-4) from each of two sheet metals (48% and 82% RT) according to ISO 6892-1 to perform Δr calculations. Tensile tests were performed with Instron 5582 Tensile Test machine with the speed of 1 mm/minute.

2.4 Magnetic Barkhausen Noise Measurement

For MBN measurements, the samples with 100 mm x 100 mm dimensions were prepared from the sheets. Measurements were made by Stresstech Rollscan μScan 500-2 equipment consisting of sensors (Figure 2-2), computer and software for data acquisition.

Magnetization voltage which regulates the applied magnetization field to the specimen was set to 5 V and resultant MBN signals were filtered and amplified by 60%. During the measurements the magnetization frequency was 125 Hz and the signals were filtered in the range of 1 to 200 kHz. Number of bursts, the parameter used for determining the number of magnetizing half cycles will be stored for signal analyses, was set as 74. The calibrations were done in the transverse direction since MBN emission is higher.
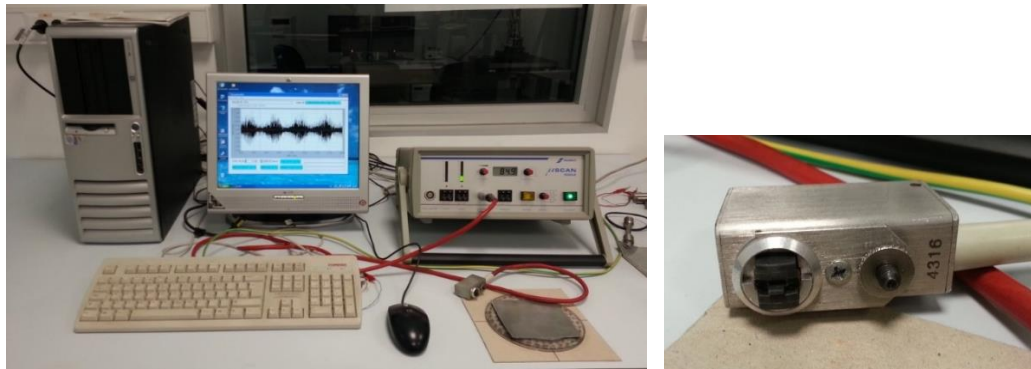
Figure 2-2 The Magnetic Barkhausen Noise device and the probe

While evaluating magnetic anisotropy in one specific point by Barkhausen noise technique, it is necessary to monitor its angular change (so-called Directional Diagram). For this aim, starting from the reference point on the surface the MBN sensor should be rotated in the radial direction with 10^0 increments until completing 360^0, and then, a polar graph is established (Figure 2-3).
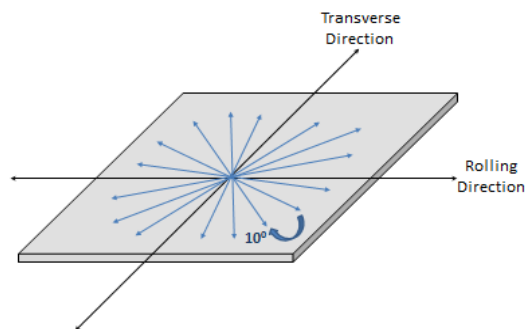
Figure 2-3 Construction of directional diagram by Barkhausen Noise measurements

2.5 Texture and Residual Stress measurement by X-Ray Diffraction Method

For X-Ray diffraction measurements, the samples with 60 mm x 60 mm dimensions were prepared from the temper rolled sheets and about 100 μm electro-polished to minimize effect of grinding.

Seifert XRD 3003 PTS system (Figure 2-4) was used to measure the texture formation in the samples. The system consists of X-Ray tube, texture-stress attachment, x-y stage, goniometer, and detector. Cr tube was used which has a wavelength of 2.28970 Å.

Figure 2-4 X-Ray system used in texture measurements

For obtaining higher statistical accuracy in texture measurements, 2 mm collimator was used in order to cover more grains. The raw pole figure data from (110), (200) and (211) planes were obtained from 1095 measurements which consist of 70 chi angle (angle between the surface normal and diffraction plane) with 5° incremental steps and 360 phi angle (rotation around the normal of the sample) with 5° incremental steps. This procedure was repeated for each plane on every sample which lasts for 18 h per sample.

For processing of the raw data, first Corrected Pole Figures (CPF) were obtained by defocussing correction, and then Normalized Pole Figures (NPF) were obtained. Inverse Pole Figures were calculated by the pole figure inversion with the help of three non-parallels pole figures (110, 200, 211).

Orientation Distribution Functions were acquired by using Triclinic to Orthorhombic Symmetrization via Inverse Pole Figures.

Since Structure Factor is equal to zero in BCC materials, (100) pole figure couldn't be measured. But, owing to the Orientation Distribution Functions, Additional Pole Figures (APF) of (100) and (111) could be calculated.

RESULTS AND DISCUSSION

3.1 Microstructural Investigation

Representative micrographs of the top and side of the samples are given in Figure 3-1 to 3-7.

Microstructural investigations show no significant amount of phases or inclusions other than ferrite. It was observed that grains elongate in the rolling direction due to cold deformation induced by temper rolling.

Figures 3-8 to 3-10 gives the SEM micrographs of the some samples, and the fracture surface of the tension test sample. It is clearly seen that there is not any additional phase or inclusions that may affect MBN measurement, except ferrite phase.

EDX analysis result performed in the grain boundary is given in Figure 3-11.
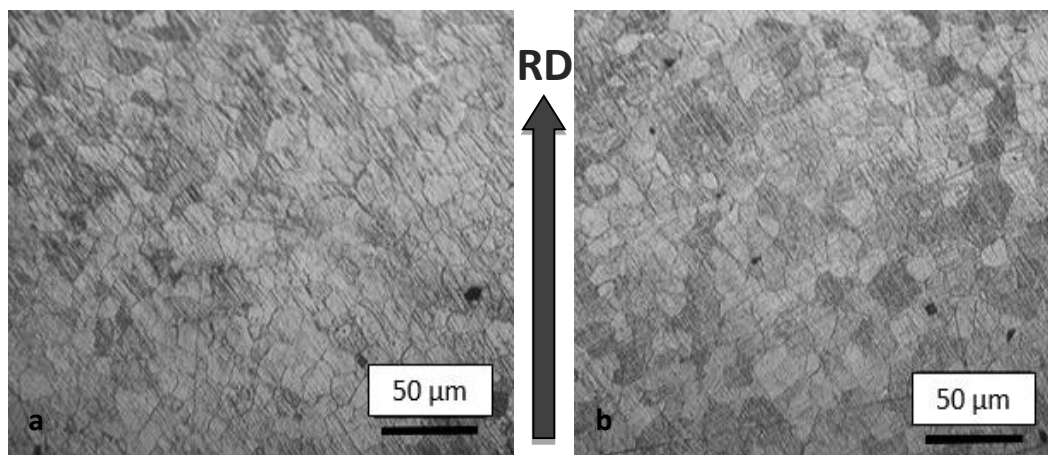
Figure 3-1(a) Top and (b) side micrographs of the normalized sample.
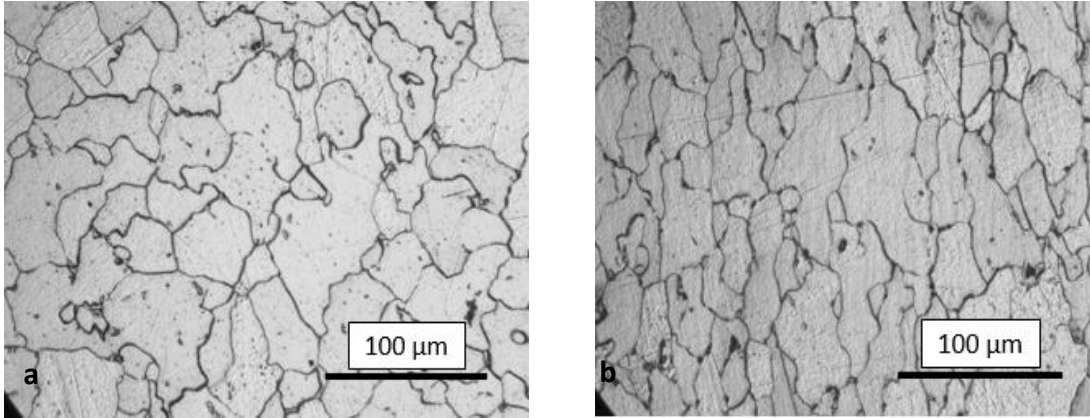
Figure 3-2 (a) Top and (b) side micrographs of the sample no 1 (48% RT)
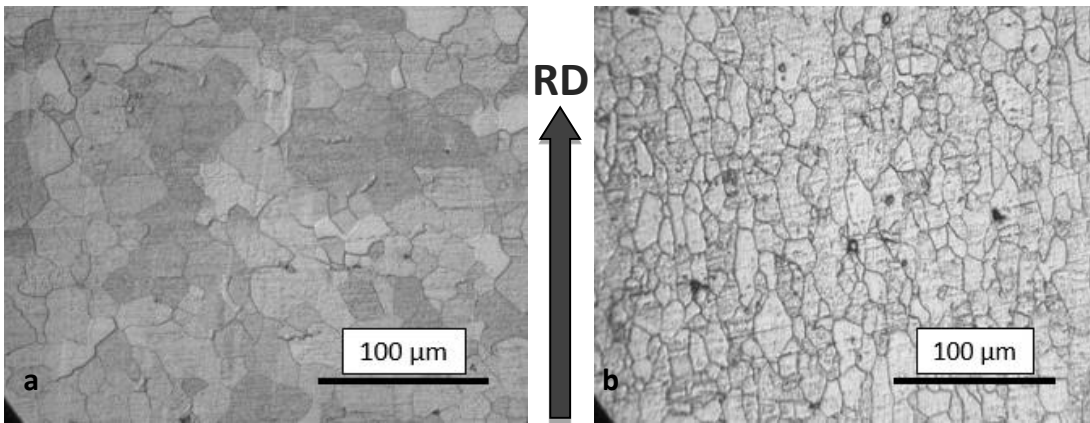
Figure 3-3 (a) Top and (b) side micrographs of the sample no 2 (56% RT)
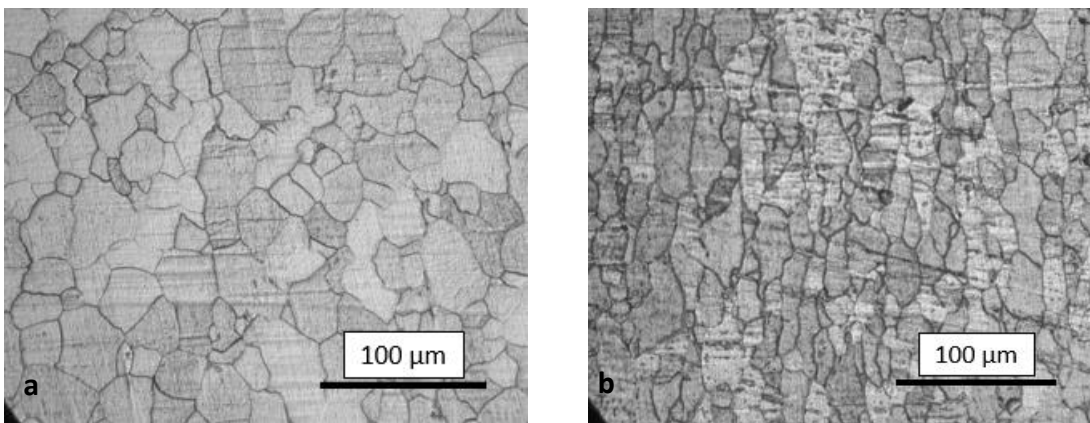
Figure 3-4 (a) Top and (b) side micrographs of the sample no 3 (64% RT)
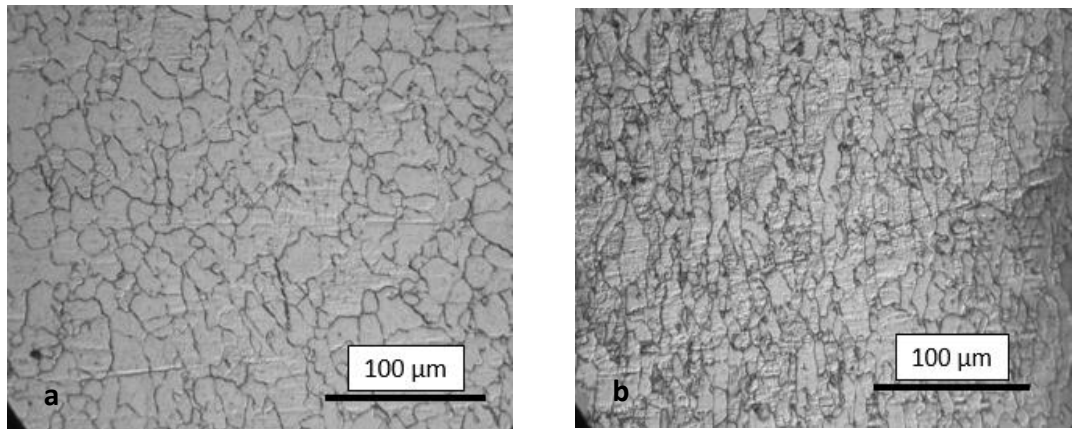
Figure 3-5 (a) Top and (b) side micrographs of the sample no 4 (73% RT)
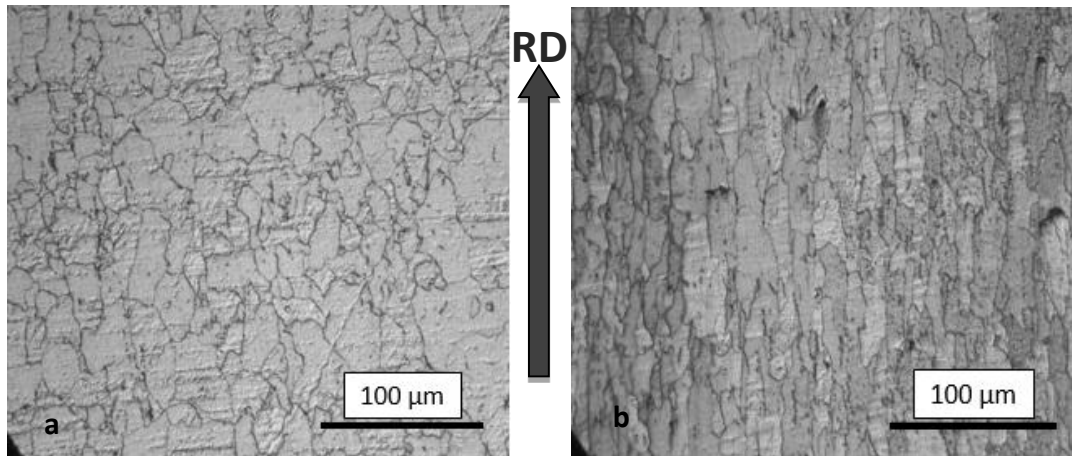
Figure 3-6 (a) Top and (b) side micrographs of the sample no 5 (77% RT)
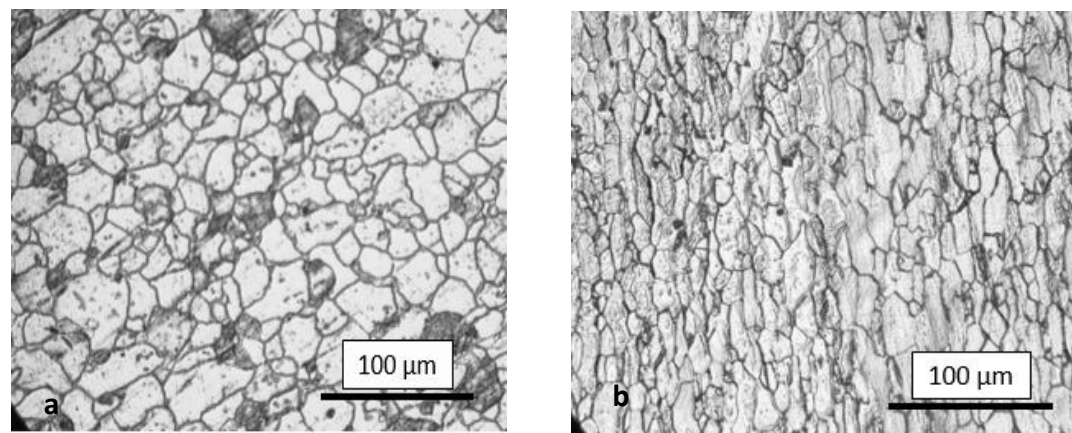
Figure 3-7 (a) Top and (b) side micrographs of the sample no 6 (82% RT)
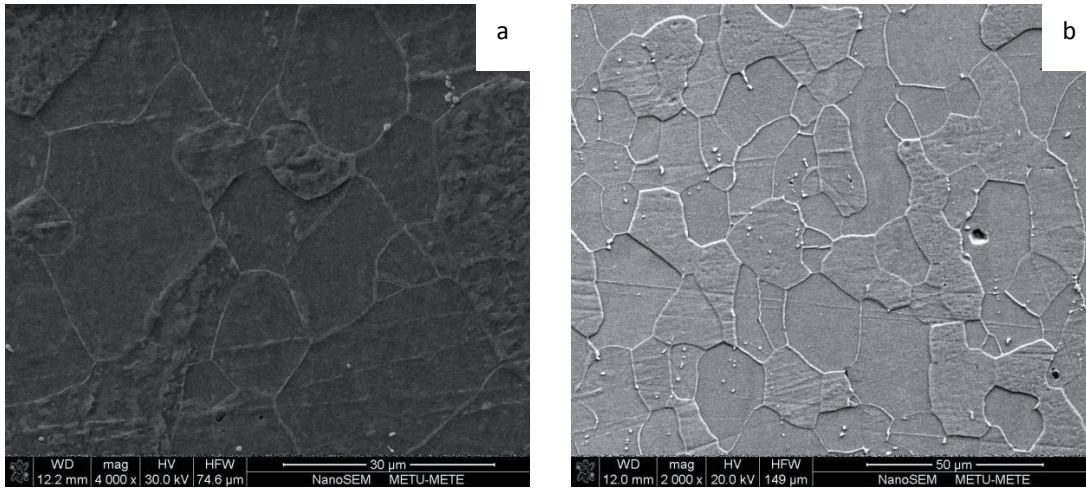
Figure 3-8 SEM (a) top and (b) side views of the sample no 5 (77% RT)
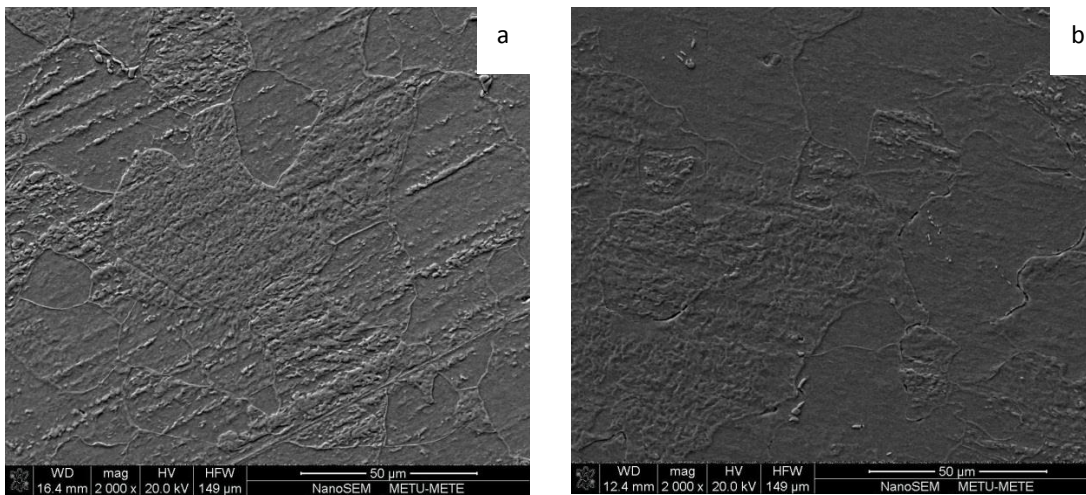
Figure 3-9 SEM top micrograph of sample no 3 (a) (64% CW) and 1 (b) (48% RT)
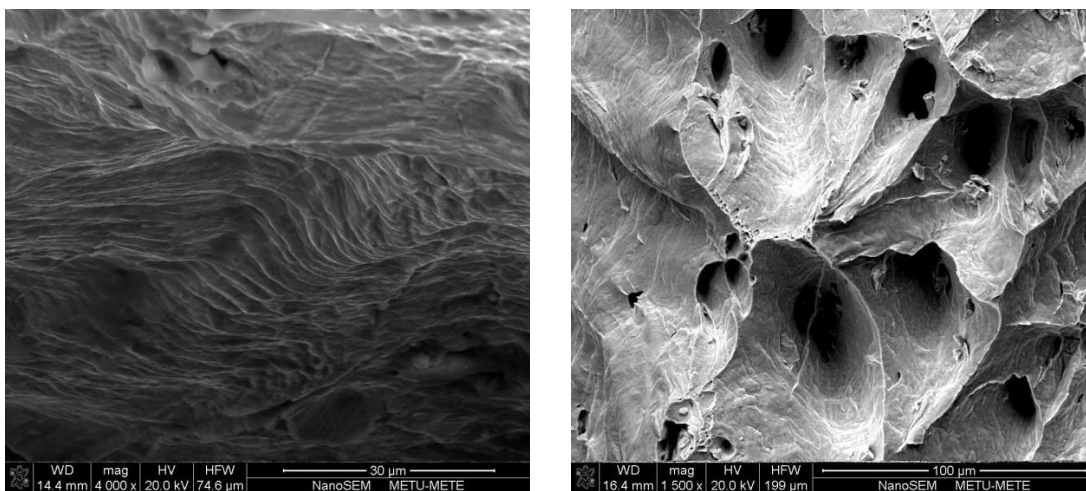
Figure 3-10 SEM micrographs of the fracture surface (tension test specimen)
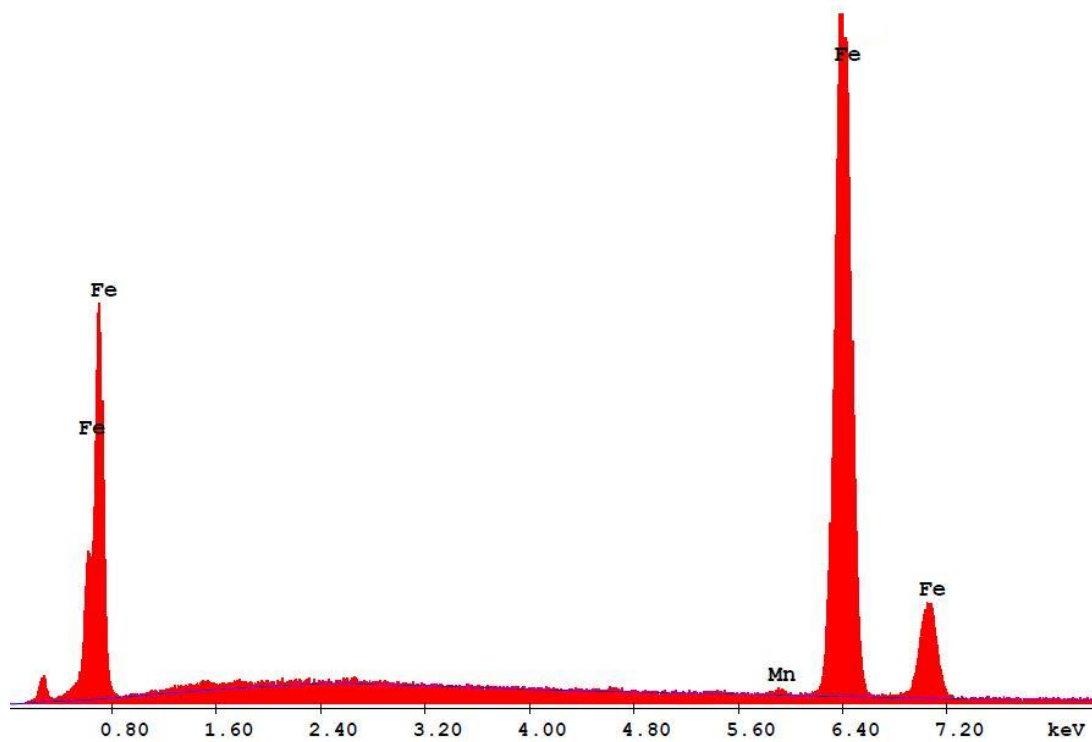
Figure 3-11 EDX-Analysis: 0.56 % Mn + 99.44 % Fe (wt %)

3.2 Grain Size Measurement Results

Results of the grain size measurements are presented in Table 3-1. It is seen that average grain size decreases with increasing % reduction in thickness due to the combined effects of skin pass rolling and subsequent annealing process. It is known that temper rolling also alters dislocation density and dislocation tangles.

Table 3-1 Average grain size of the samples

Sample No	% RT	Average Grain Size (±7 μm)	
		Top	Side
1	48	42	35
2	56	27	20
3	64	28	20
4	73	22	15
5	77	23	15
6	82	20	16

3.3 Results of Hardness and Tension Tests

Results of the hardness measurements are given in the Figure 3-12. It is clearly seen that hardness values are almost the same for all samples due to annealing during deformation process. Results of the tensile tests applied to the 48% RT and 82% RT are given in the Table 3-2. The yield strengths of the samples are close to the upper limit given in ASTM A1008 (115 to 200 MPa). The strength values are slightly higher for 82% RT sample. Besides, the tensile strengths are slightly higher in the direction that is 45^0 to the rolling direction.
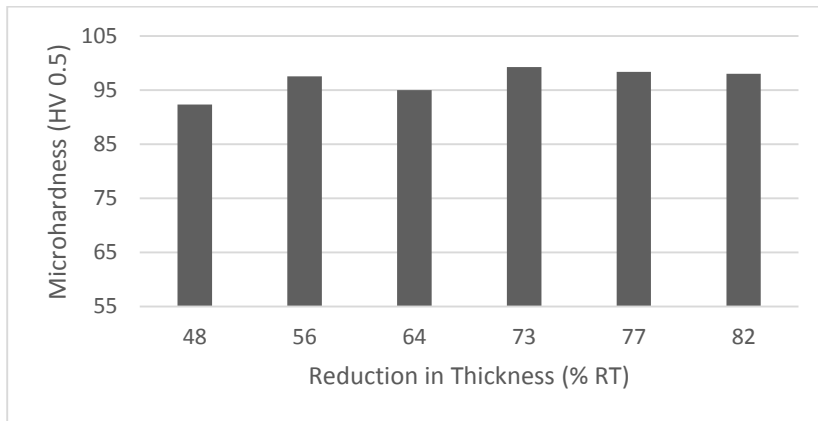
Figure 3-12 Average micro-hardness values of the samples

Table 3-2 Tensile test results

	YP (MPa)			UTS (MPa)			%El			Δr
	0^0	45^0	90^0	0^0	45^0	90^0	0^0	45^0	90^0	
48% RT	186	202	189	292	296	291	54	49	54	0.27
82% RT	192	203	199	299	306	300	39	39	41	0.17

3.4 Residual Stress Measurement Results

The surface residual stresses, measured by X-Ray diffraction method, on the 48%, 64% and 82% RT samples are given in Table 3-3. Results show that for all samples, compressive residual stresses exist on the surface, and their magnitudes in the transverse direction are higher than those in the rolling direction.

Table 3-3 Surface residual stress values obtained by X-Ray diffraction

	RD (MPa)	TD (MPa)
48% RT	-75	-85
64% RT	-60	-74
82% RT	-89	-108

28

3.5 X-Ray Texture Measurement Results

{100}, {110}, {111} and {211} pole figures were subtracted for the texture characterization. Pole figures obtained by X-ray diffraction measurements are given in Figures 3-14 to Figure 3-19, in the sequence of increasing %RT.

When % reduction in thickness steps up on to 60% in a low carbon steel sheet, <111> γ-fibering parallel to the normal direction happens. On the other hand, X-ray measurements showed that when the thickness reduction scales up, an increase is seen in <111> texture level which are parallel to the normal direction and which are making 45^0 together with normal and rolling direction. The only exception is a small decrease in the sample which has the maximum deformation.

Another expected texture component is <110> α-fibering that is parallel to the rolling direction. In a confirmatory nature, with the increase in the amount of thickness reduction, <110> level linear also increases. Yet another texture parallel to the rolling direction is {112} α-fibering. As observed in the results, this component enhances with the amount of deformation; however, it remains low in comparison to other fiberings.

The texture component which plays a major role in the formation of Barkhausen noise is <100>. It is a magnetically favorable direction for the materials having BCC crystal structure. Magnetic easy direction is expected to change with the change in the intensity of <100>.

<100> shows a parallel formation to the rolling direction, and makes an angle of 45^0 with the normal axis of the sheet. It can be said that the highest intensities of <100> direction perform 90^0 wall motion (Figure 3-13) which has lower domain wall energy [47].
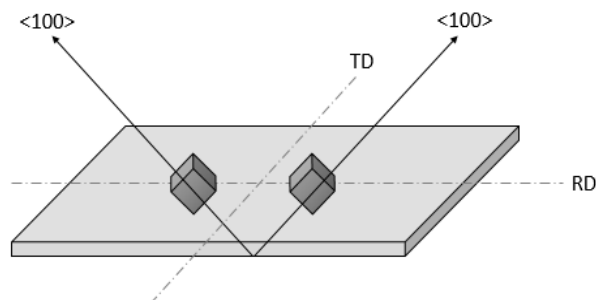
Figure 3-13 90^0 domain wall formation in the <100> direction

Pole figure shows that for the lowest deformation rate (48% RT) <100> intensity is higher in the transverse direction than in the rolling direction. However, as reduction ratio increases, higher intensity region of <100> component shifts from the transverse direction to the rolling direction; and causes an increase in <100> texture in the rolling direction.
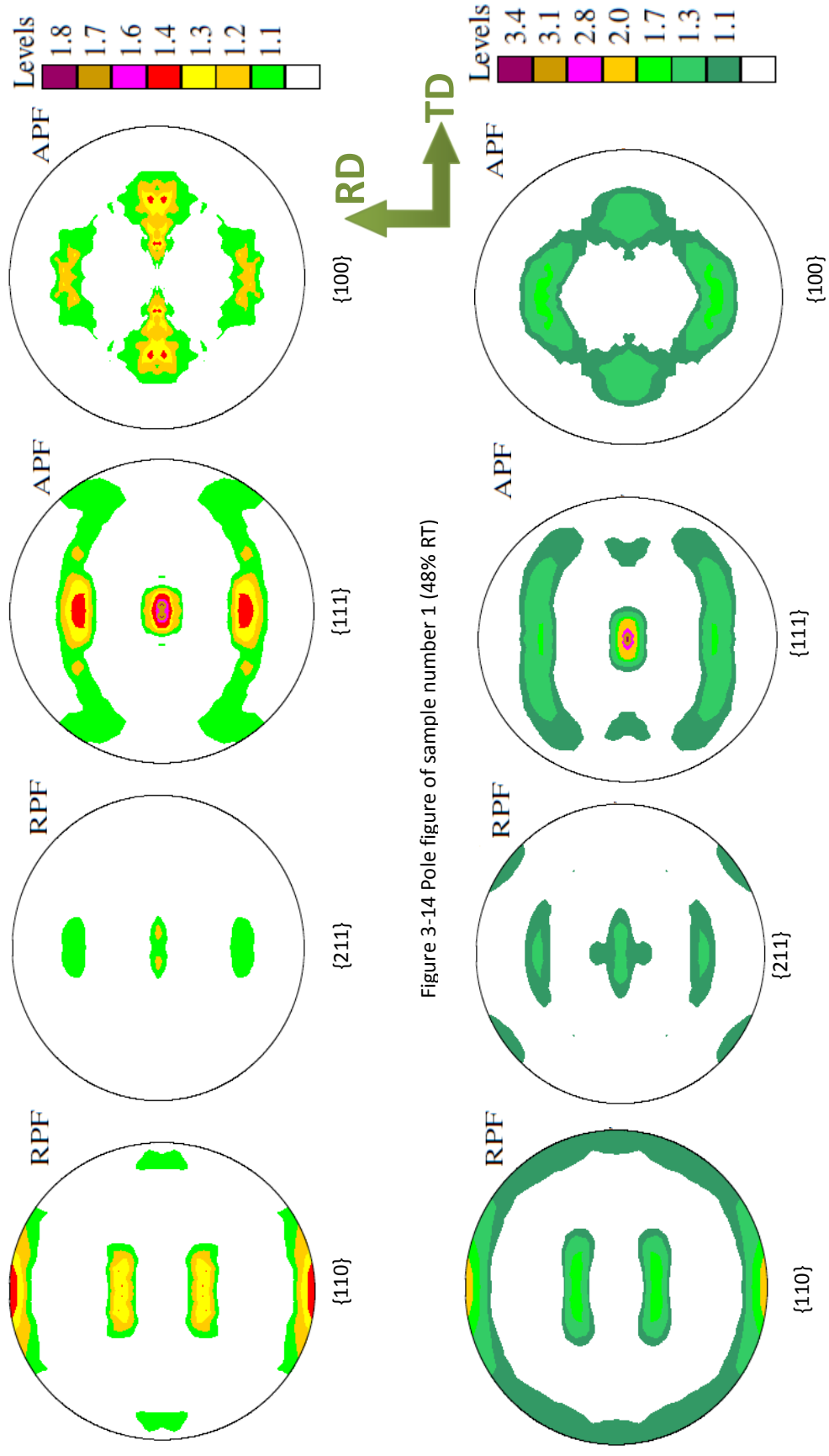
Figure 3-14 Pole figure of sample number 1 (48% RT)

Figure 3-15 Pole figure of sample number 2 (56% RT)
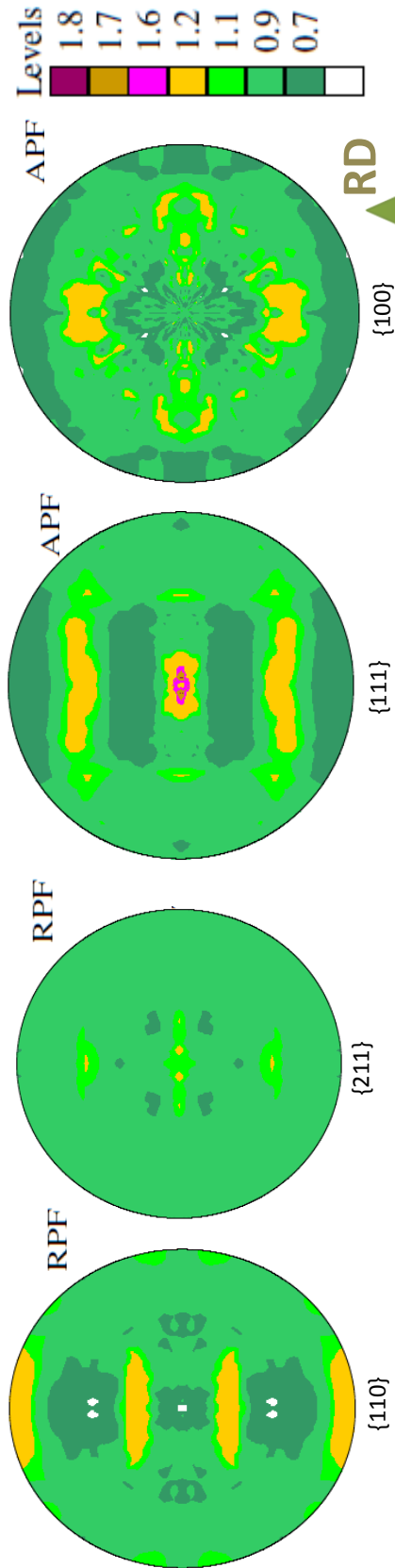
Figure 3-16 Pole figure of sample number 3 (64% RT)
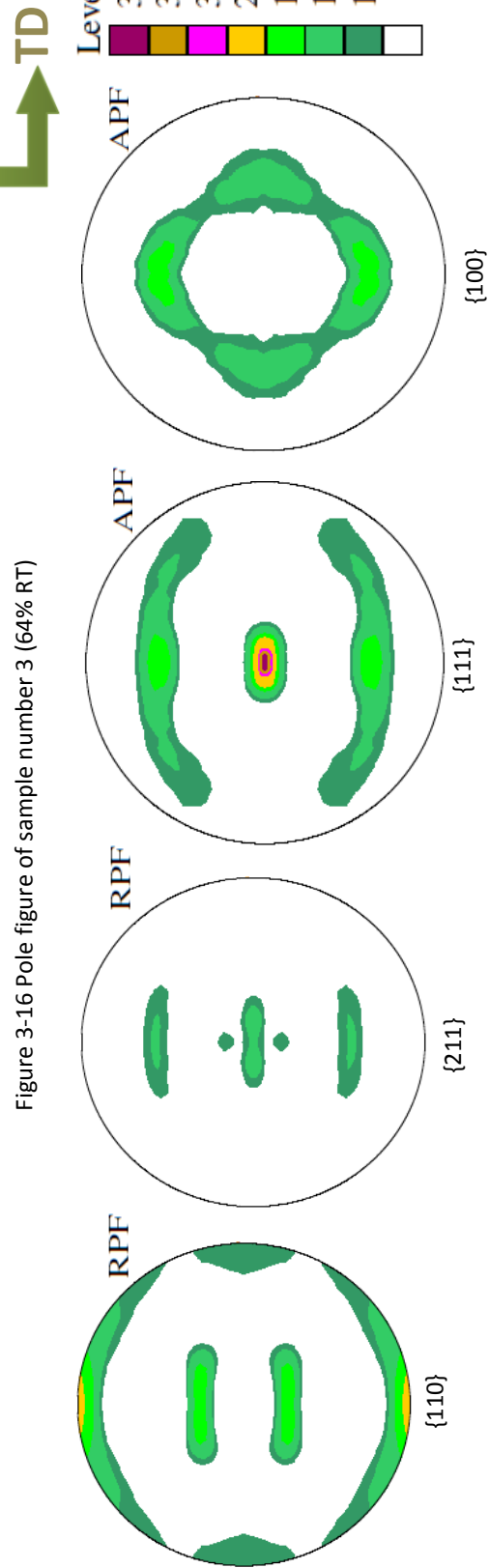
Figure 3-17 Pole figure of sample number 4 (73% RT)

31

Levels
6.3
5.7
5.0
3.1
2.5
1.6
1.4

APF

APF

RPF

RPF

{100}

{111}

{211}

{110}

RD

TD

Figure 3-18 Pole figure of sample number 5 (77% RT)

Levels
5.2
4.7
4.2
2.7
2.3
1.5
1.3

APF

APF

RPF

RPF

{100}

{111}

{211}

{110}

Figure 3-19 Pole figure of sample number 6 (82% RT)
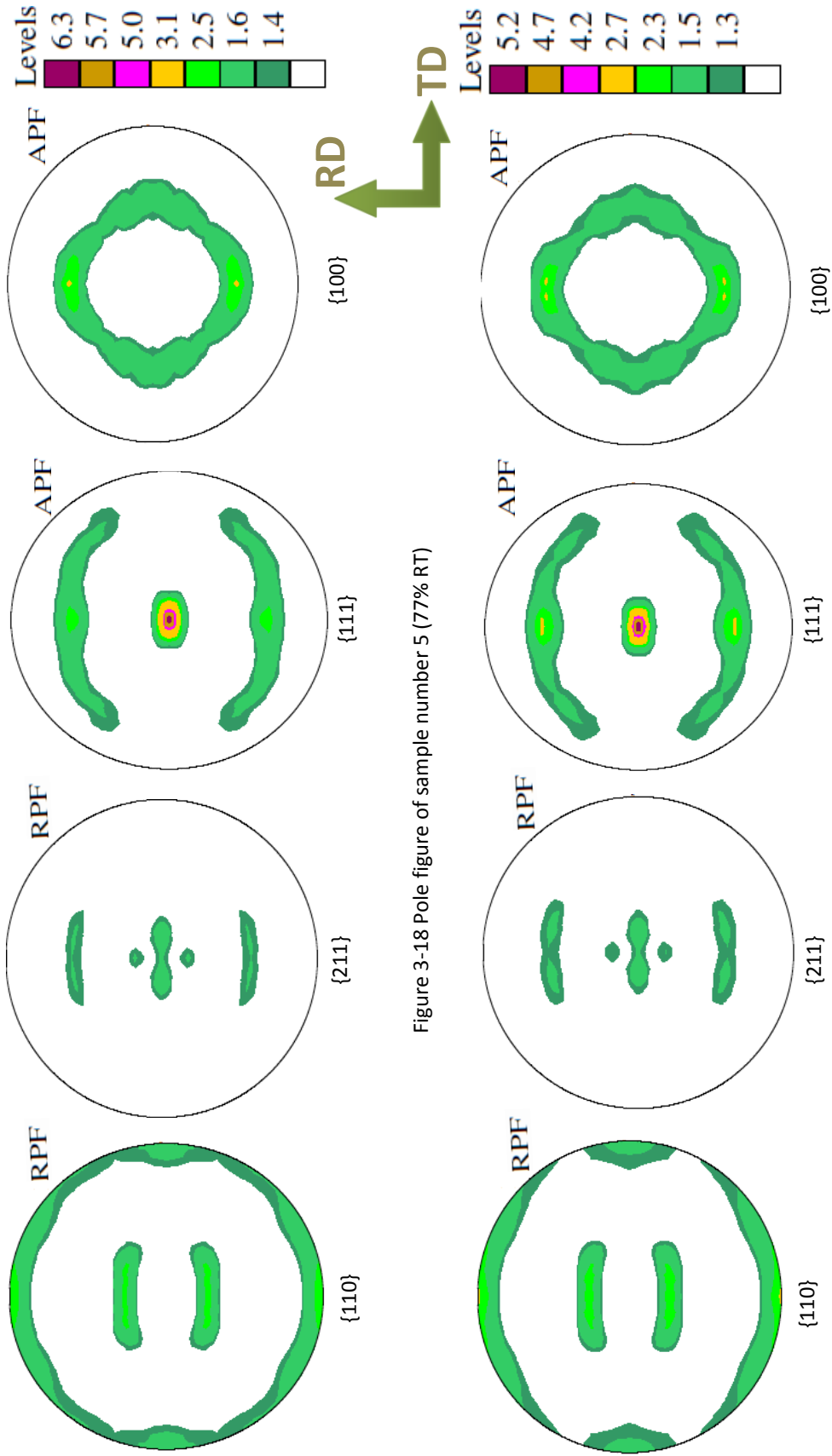
3.6 Results of Magnetic Barkhausen Noise Measurements

3.6.1 Roll Scan Results

3.6.1.1 Temper Rolled Samples

It is known that any change in the average grain size alters the MBN activity. The inverse relationship between grain size and MBN emission is observed in accordance with Equation 1-11; i.e., MBN emission increases with decreasing grain size (Figure 3-20).
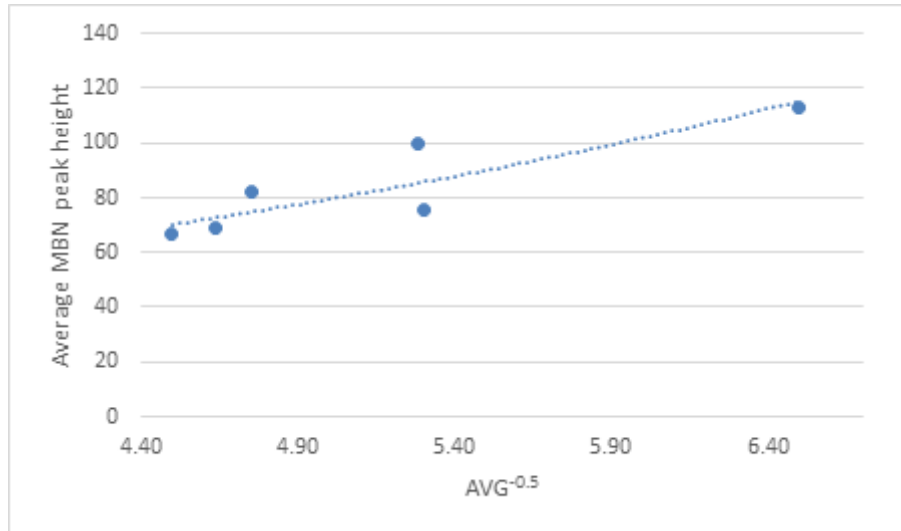
Figure 3-20 Relation between MBN peak height and average grain size

The best way for prediction of the magnetic anisotropy in the deformed low-C steel samples is the construction of the Directional Diagram based on the MBN measurements.

The Directional Diagrams of the temper rolled samples are given in Figure 3-21, and that of the normalized sample is given in Figure 3-22; (All experimental data are given in the Appendix A).

A clear relationship between magnetic anisotropy and % reduction in thickness was observed. After %48 reduction in thickness, the magnetic easy axis is parallel to the transverse direction. After 64% reduction in thickness, the sheet becomes magnetically isotropic, i.e. no significant magnetic easy axis exists. For 73% RT sample the magnetic easy axis becomes parallel to the transverse direction, again. However, if % reduction in thickness is increased further, easy magnetization direction starts to disappear and the material acts as magnetically isotropic.

The change in the rate of $MBN_{energy-ratio}$ that is important to explain the variation in the magnetic anisotropy is presented in Figure 3-23. It shows partial similarities with the results of Stefanita et al [13]. They reported that magnetic easy direction is parallel to the transverse direction for 40% deformation, however, for deformation ratios higher than 60%, a contradiction occurs and magnetically favorable direction do not shift to the rolling direction.

The average values of the Barkhausen emission for all directions are given in Figure 3-24 in order to see the overall effect of deformation.
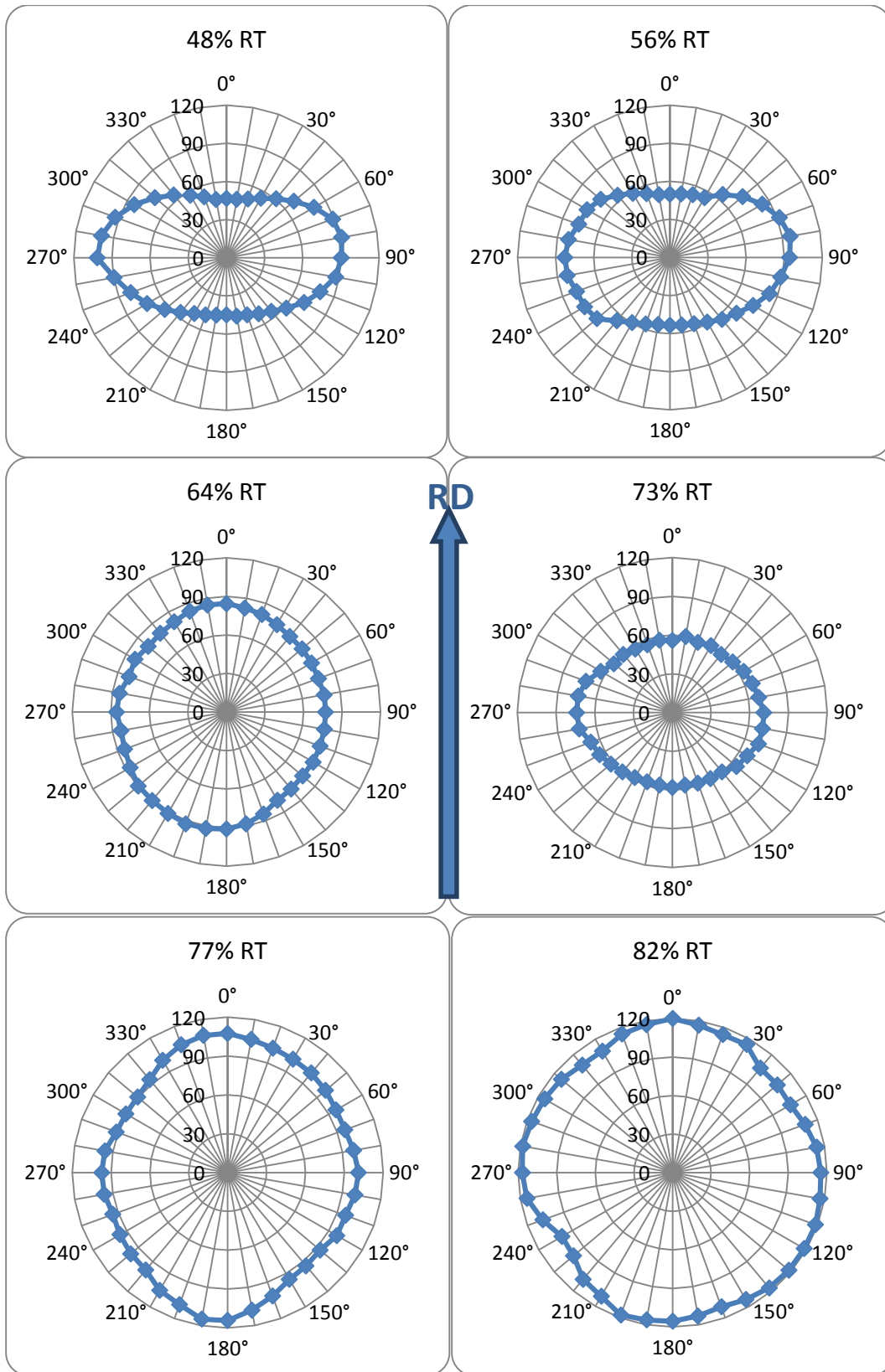
Figure 3-21 MBN directional diagrams of the temper rolled samples
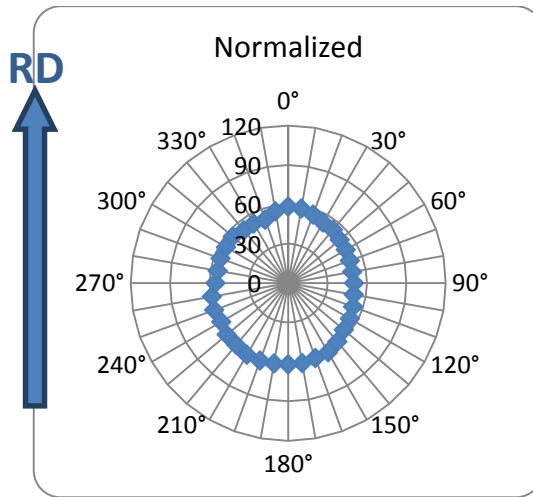
Figure 3-22 MBN directional diagram of the normalized sample (850^{0}C/1 h; air cooling)
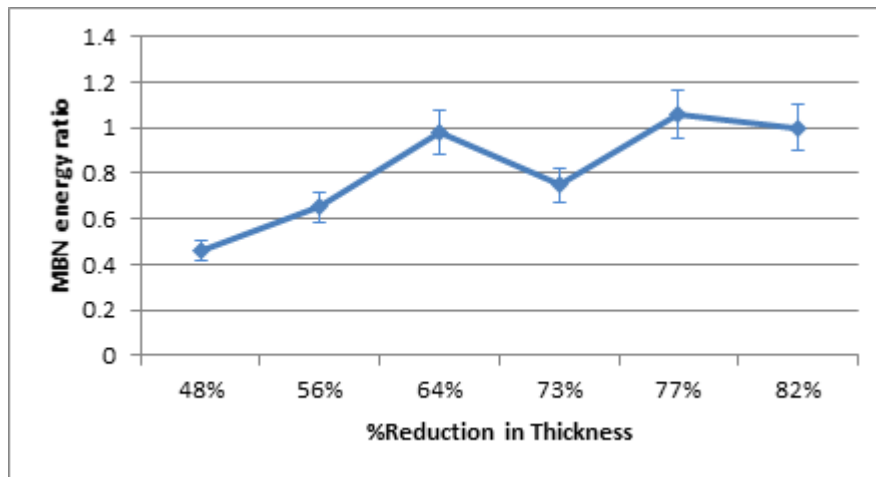
Figure 3-23 Variation of MBN$_{energy\ ratio}$ with % reduction in thickness
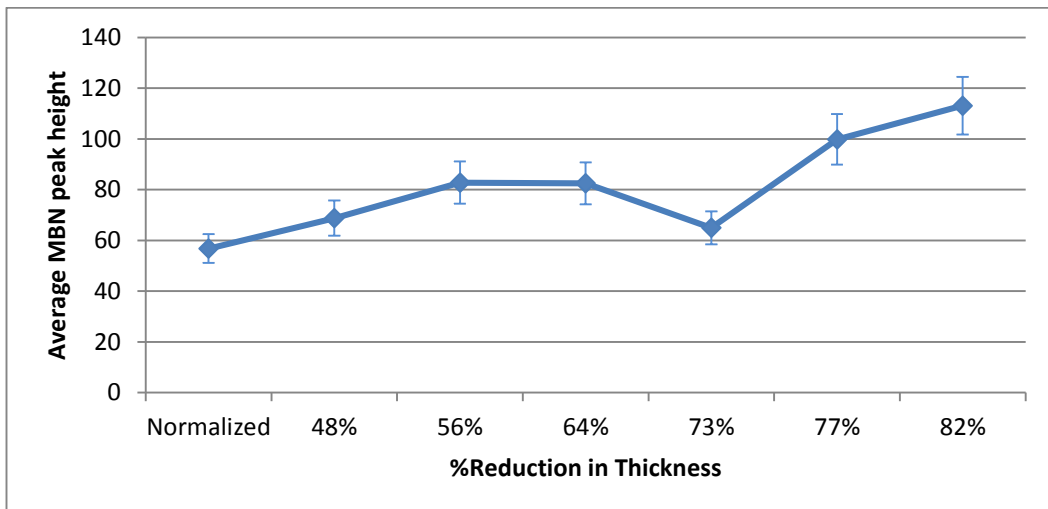
Figure 3-24 Variation of average MBN peak height with % reduction in thickness

3.6.1.2 Stress Relieved Samples

The purpose of the stress relief heat treatment was to eliminate the effect of residual stress on the magnetic anisotropy in the sheet metal.

In the stress relieved samples, a change in the easy axis direction was observed (Figure 3-25). When the amount of deformation increases up to 50% the magnetically favorable direction rotates from the transverse direction to the rolling direction. Based on this, MBN $_{energy\ ratio}$ and average MBN emission are expected to show the similar tendency with increasing % reduction in thickness (Figure 3-26 and 3-27).

In Figures 3-28 and 3-29, the results for the temper rolled and the stress relieved samples are given in the same graphs to clearly observe the change in magnetic anisotropy.

The relationship between MBN emission and percent reduction in thickness obtained in this study supports the results of Liu et al. [48]. They reported that MBN energy and MBN rms voltage increase with increasing rolling ratio up to 20%, whereas in this study, MBN peak height increases with increasing reduction ratio. Moreover, as it is seen in Figure 3-30, average MBN emission in the stress relieved samples shows a significant decline in comparison with the temper rolled samples. The reason of this decline seems to be the decrease in the number of domain nucleation and pinning sites, i.e. dislocation tangles.
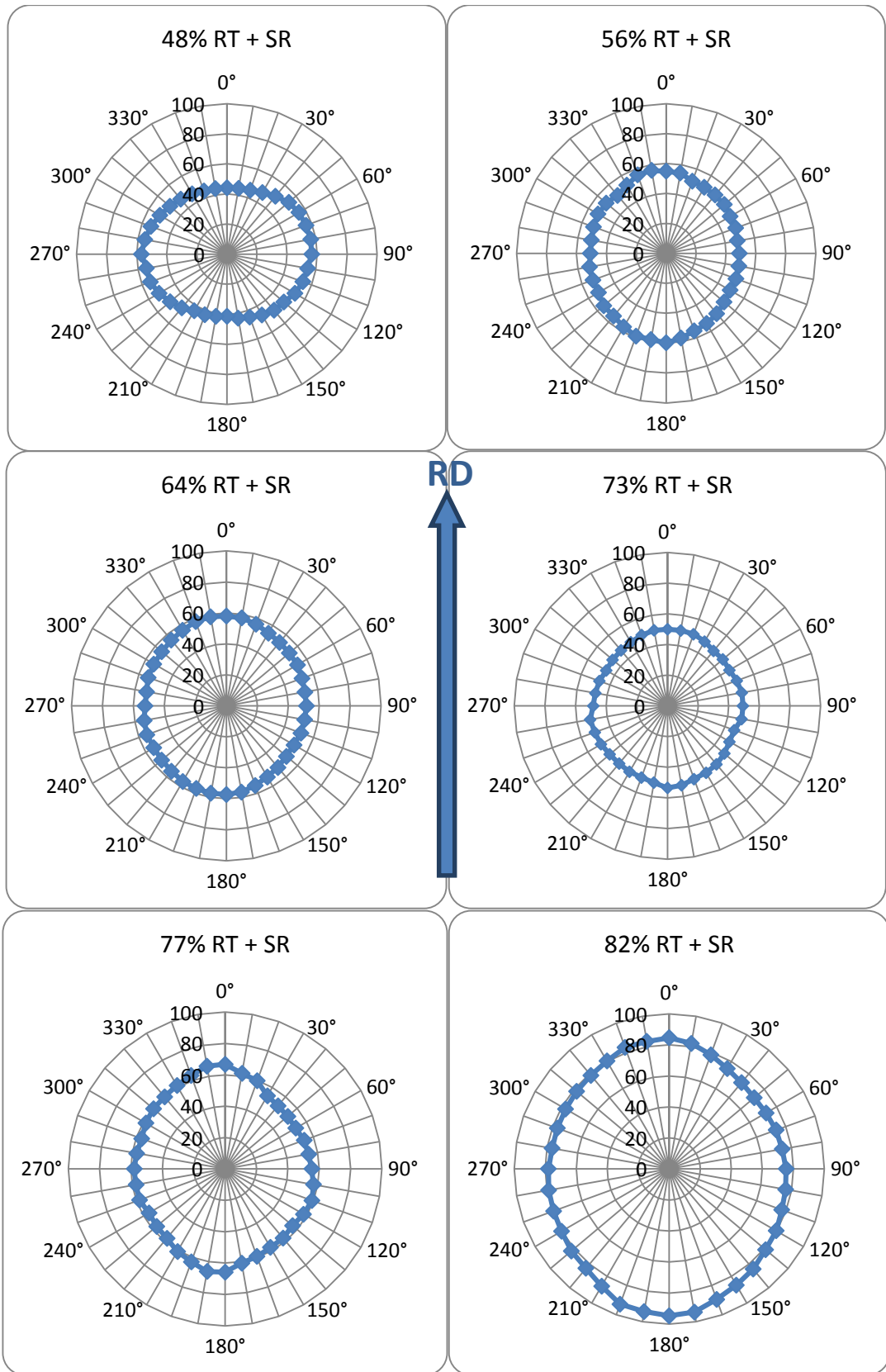
Figure 3-25 MBN directional diagrams of the stress relieved samples (500^0C/1 hr)
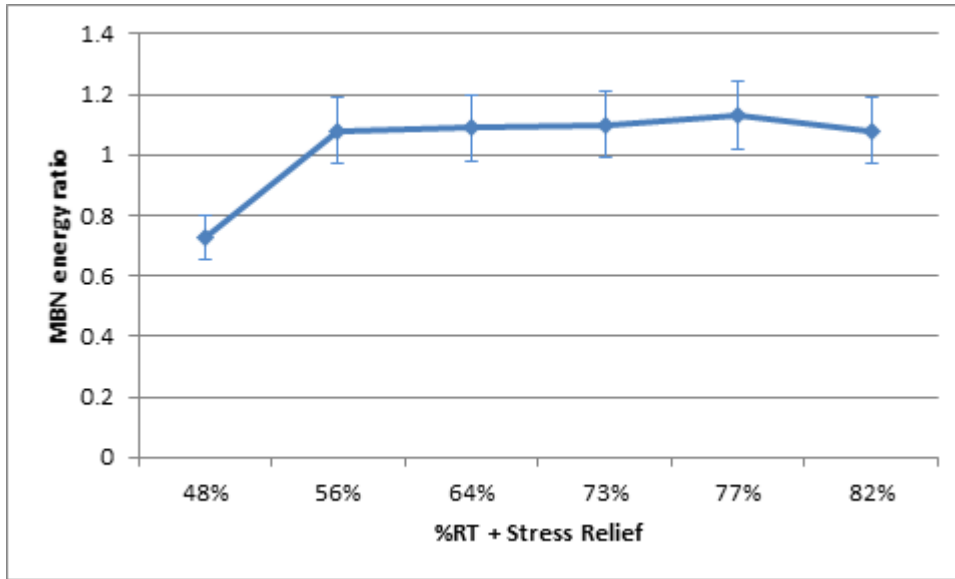
Figure 3-26 Variation of MBN $_{energy\ ratio}$ with % reduction in thickness (stress relieved samples)
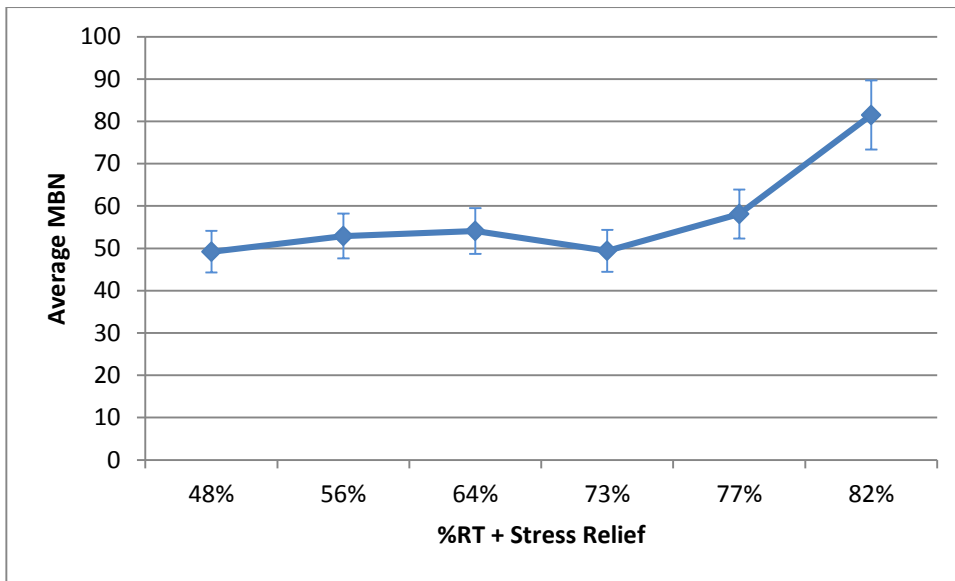
Figure 3-27 Variation of average MBN emission with % reduction in thickness (stress relieved samples)
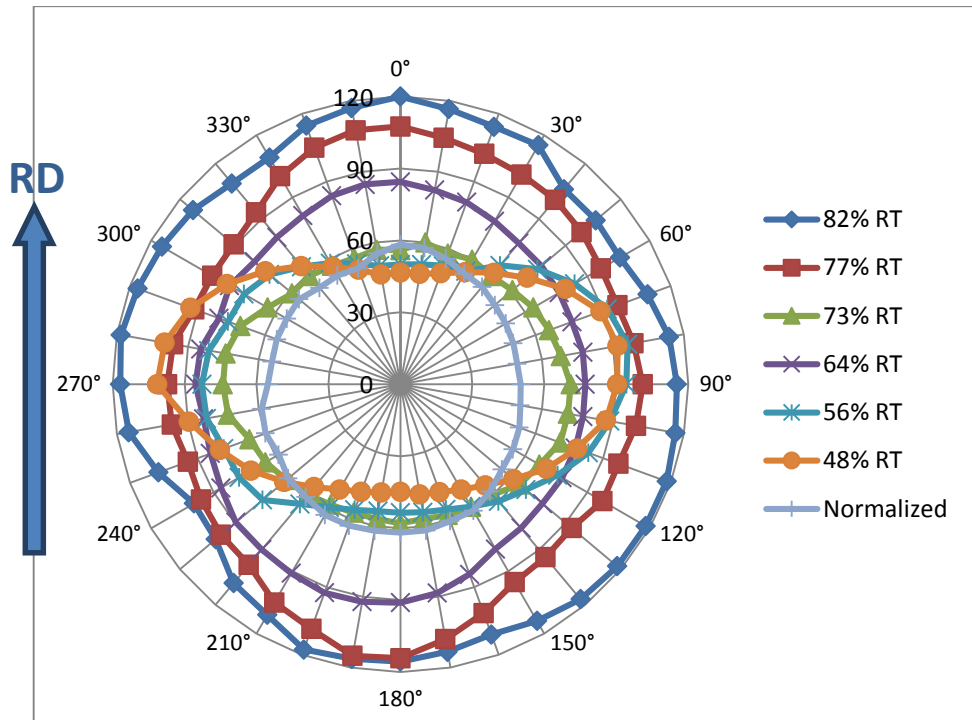
Figure 3-28 Combined MBN directional diagram of the temper rolled samples
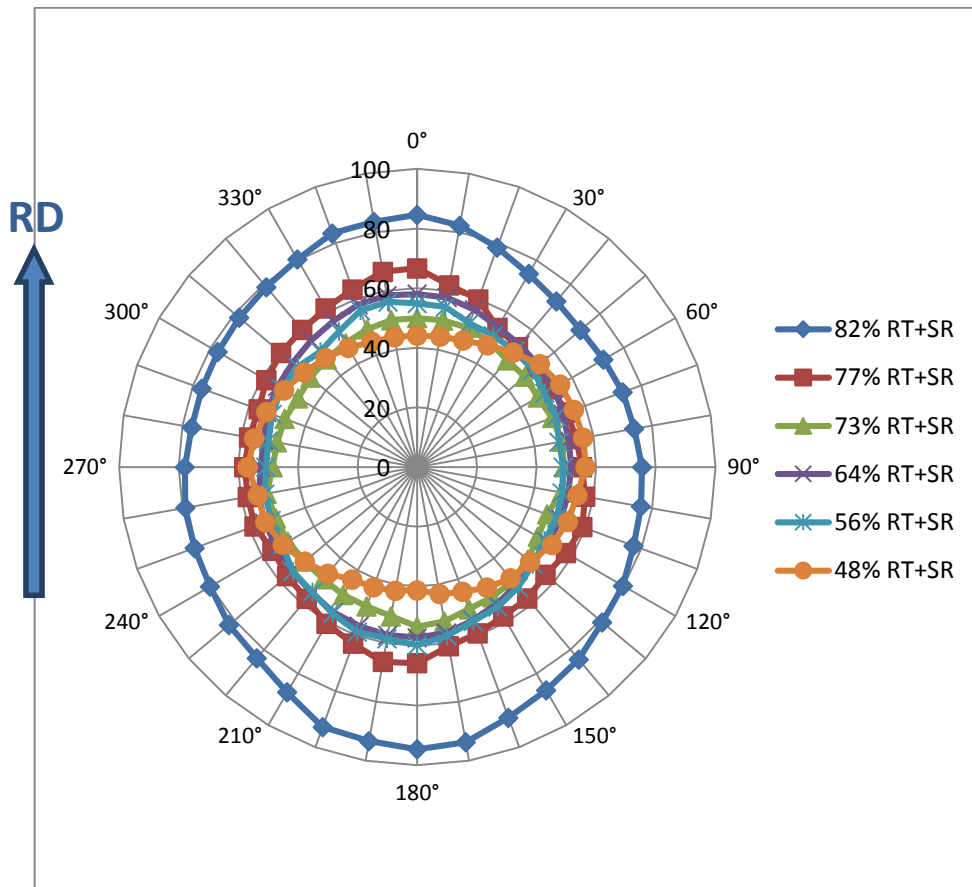
Figure 3-29 Combined MBN directional diagram of the stress relieved samples
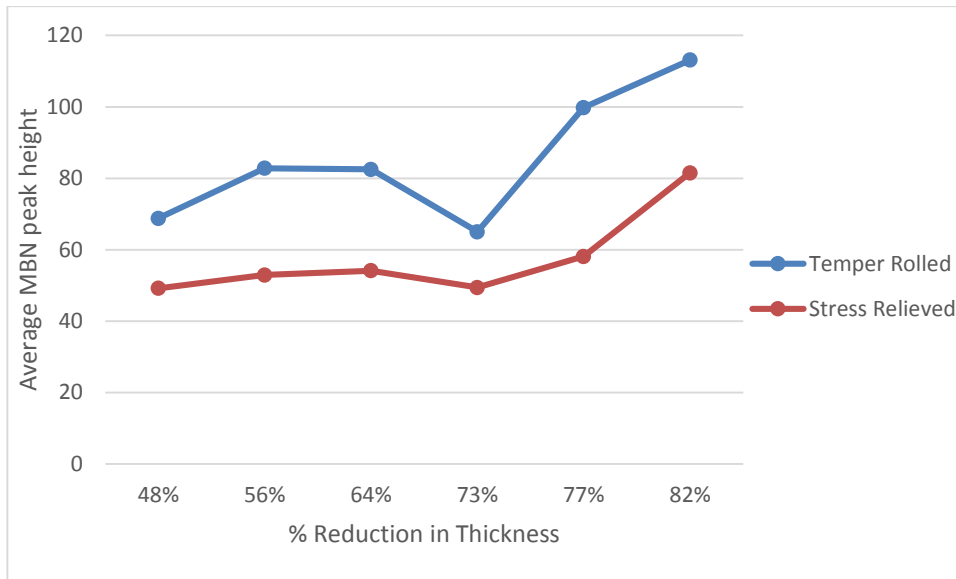
Figure 3-30 Average MBN emission values of the temper rolled and the stress relieved samples (independent upon direction)

For a better understanding of the variation in the magnetic easy direction and average MBN emission with stress relief treatment, the combined directional diagrams are given in Figure 3-31. Magnetic easy direction appears to be parallel to the transverse direction for the 48%, 56% and 73% RT samples. On the other hand, for the stress relieved samples, magnetically favored direction is parallel to the rolling direction except the sample no 1 (48% RT+SR) which has magnetic easy axis in the transverse direction as shown in Figure 3-32.
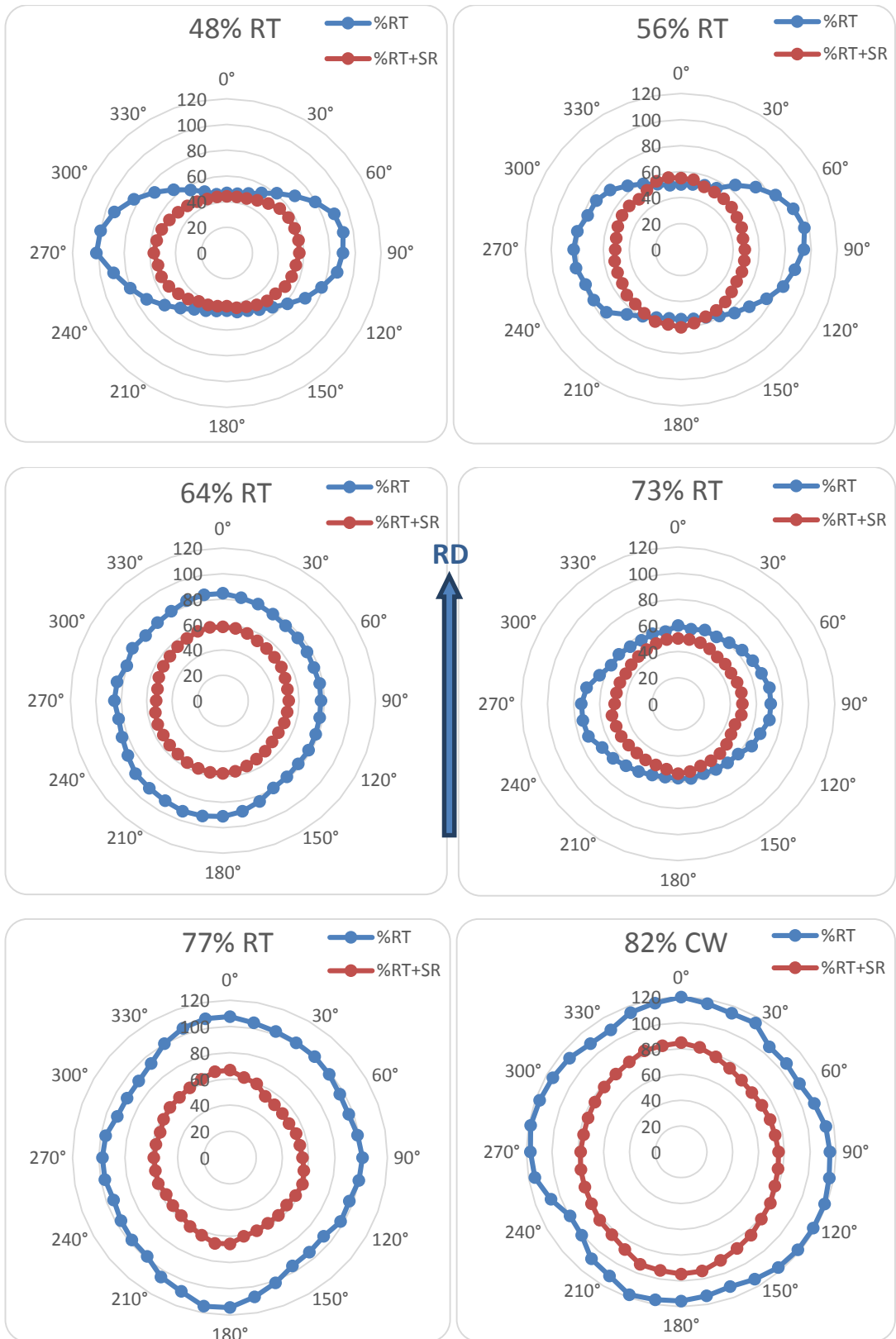
Figure 3-31 Combined MBN Directional Diagrams of the temper rolled and the stress relieved samples
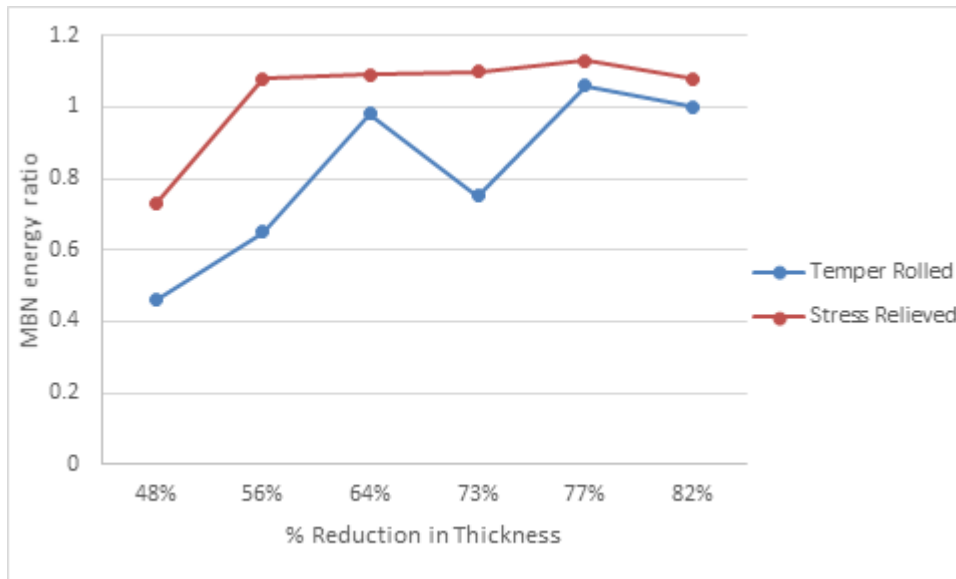
Figure 3-32 MBN energy ratios of the temper rolled and the stress relieved samples

The anisotropy in magnetic properties can be explained in two different ways. First, as it is seen in pole figure data (Figure 3-14 to 19), magnetically hard axis, <111>, has its highest texture components in the normal direction and the direction that is 45^0 to the rolling direction. It hinders the domain wall motion which results in lower MBN emission in the rolling direction, and leads the formation of magnetic easy direction parallel to the transverse direction. The second explanation might be the dominant influence of strain hardening on the formation of Barkhausen noise in the deformed samples. The number of pinning sites induced by plastic deformation is higher in the transverse direction than those in the rolling direction. Therefore, higher MBN emission occurs in the transverse direction.

Effect of texture on MBN results can be directly observed after relieving residual stresses. In terms of the <100> intensity of the sample no 1 is more profound in the transverse direction. It is also seen from MBN$_{energy-ratio}$ that the sample exhibits anisotropic magnetic behavior because of texture component. But, for higher thickness reductions, there is an increase in the intensity of <100> in the rolling direction. Its combined effect with the low energy 90^0 wall motion, magnetic easy axis shifts from the transverse direction to the rolling direction. It is revealed that magnetic easy axis direction remains as it is up to 82% reduction. Moreover, <110> plane exhibits a similar behavior and while deformation ratio raises its intensity increases in the rolling direction. Thus, it can be concluded that combined effect of <100> and <110> texture formation seems to be dominant on the shift of the magnetic easy direction.

3.6.2 μ-Scan Results

3.6.2.1 MBN Fingerprint

MBN signal versus applied field strength graphs (MBN fingerprint) for the rolling and transverse directions are given in Figure 3-33 and 3-34, respectively. There are two impacts of the increase of % reduction: the increase in the necessary quantity of applied field to reach the maximum MBN level and the increase in MBN peak height depending upon % deformation. The unexpected behavior in these results is that MBN peak height of the 48% RT sample is higher than that of 73% RT sample in the transverse direction both for the deformed and the stress relieved samples. However, relative magnetic field strength of 48% RT sample is found as it is expected. The temper rolled samples have higher RMS voltage than the stress relieved and the normalized samples.

a   b
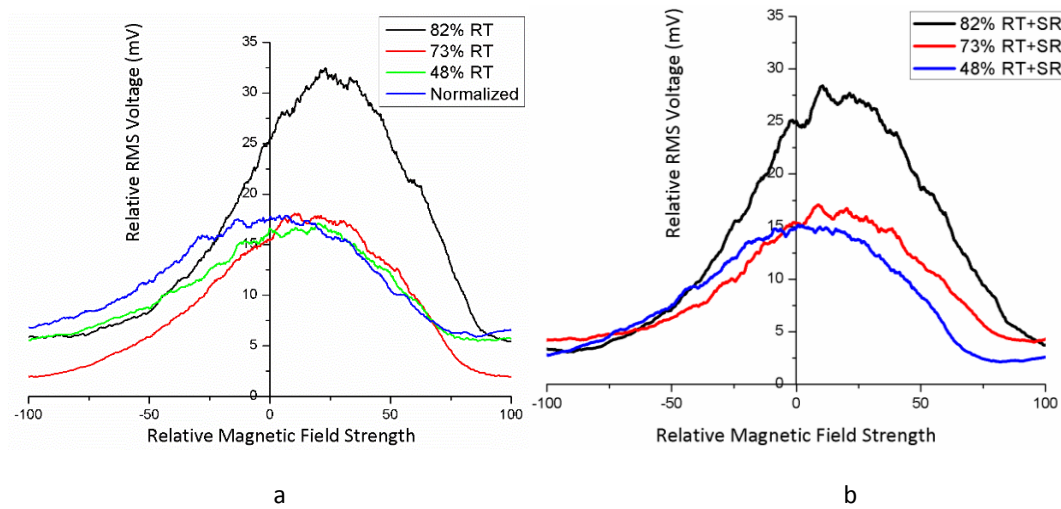
Figure 3-33 MBN fingerprints in the rolling direction a) temper rolled (%RT), b) stress relieved (%RT+SR)

a   b
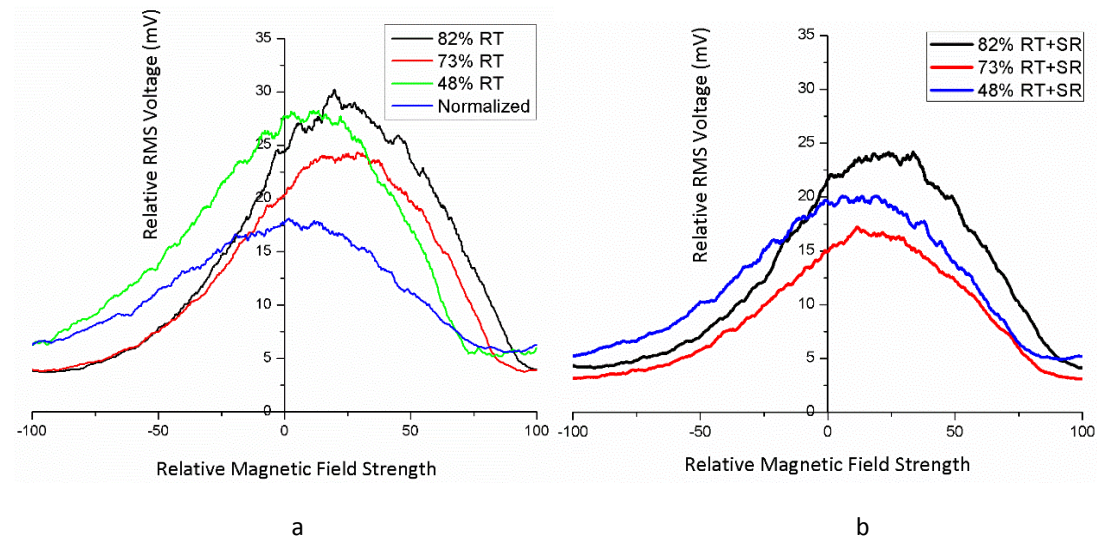
Figure 3-34 MBN fingerprints in the transverse direction a) temper rolled (%RT), b) stress relieved (%RT+SR)

The µScan results confirm the magnetic anisotropy variations detected by the Roll Scan measurements. The peak heights of MBN fingerprints increase with increasing % reduction. The reason seems to be the shortening of the mean free paths of domain walls due to grain size reduction and subcell formation [2]. In addition, since deformation makes the materials harder, a higher magnetic field is required to reach saturation. Thus, for low thickness reductions, peak value shifts to the left; i.e. lower magnetic fields.

48 % and 73% RT samples have higher RMS values in the transverse direction, while 82% RT sample behaves magnetically isotropic and have the same RMS values in the rolling and transverse directions. For the stress relieved samples, while 48% RT+SR sample has a higher MBN peak in the transverse direction, 73% and 82% RT+SR samples have higher RMS values in the rolling direction.

The magnetic behavior of the normalized sample is isotropic. Since recrystallization causes remarkable reduction in the number of pinning sites for domain motion, the magnetic field strength requirement is much lower than that for the temper rolled samples, i.e. close to zero.

3.6.2.2 Frequency Spectrum

To determine the spectral content of time domain signals, time domain of raw MBN data can be replaced with frequency domain by applying Fourier transformation. Figure 3-35 and 3-36 show the frequency spectrum of the temper rolled samples, the normalized and the stress relieved samples in the rolling and transverse directions, respectively.

While the positions of the MBN peaks remain unchanged, their amplitudes increase in accordance with % reduction in thickness, with the exception of the transverse direction of the 48% RT sample; and they decrease after stress relief heat treatment or normalizing heat treatment.

Frequency spectrums of both sample series show the similar tendency. The 48% and 73% temper rolled samples have higher MBN amplitudes in the transverse direction while 82% sample behaves magnetically isotropic. For the stress relieved series, 48% RT+SR specimen has a higher MBN amplitude in the transverse direction while 73% and 82% RT+SR samples have higher MBN signal amplitude in the rolling direction. The normalized sample has an isotropic frequency spectrum with moderate MBN signal amplitude as it is expected.

a   b
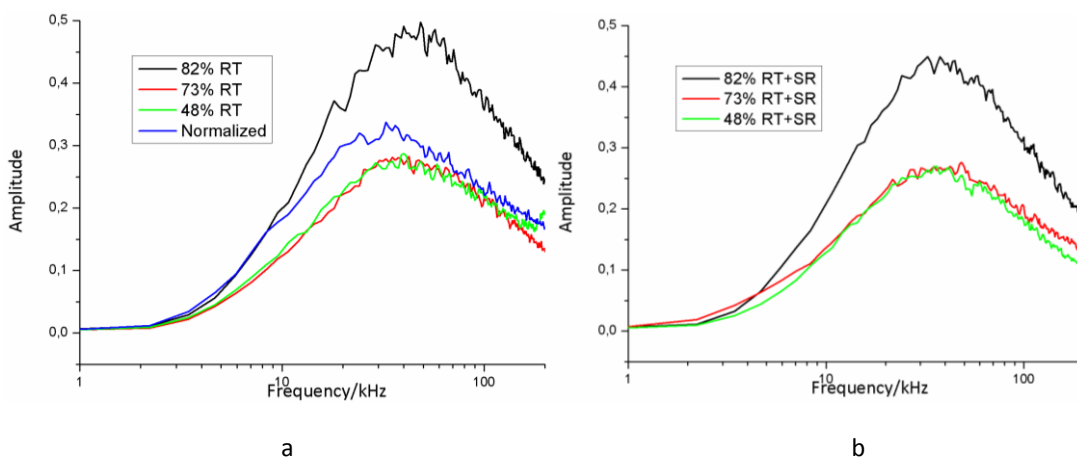
Figure 3-35 MBN frequency spectrums in the rolling direction a) temper rolled (%RT), b) stress relieved (%RT+SR)
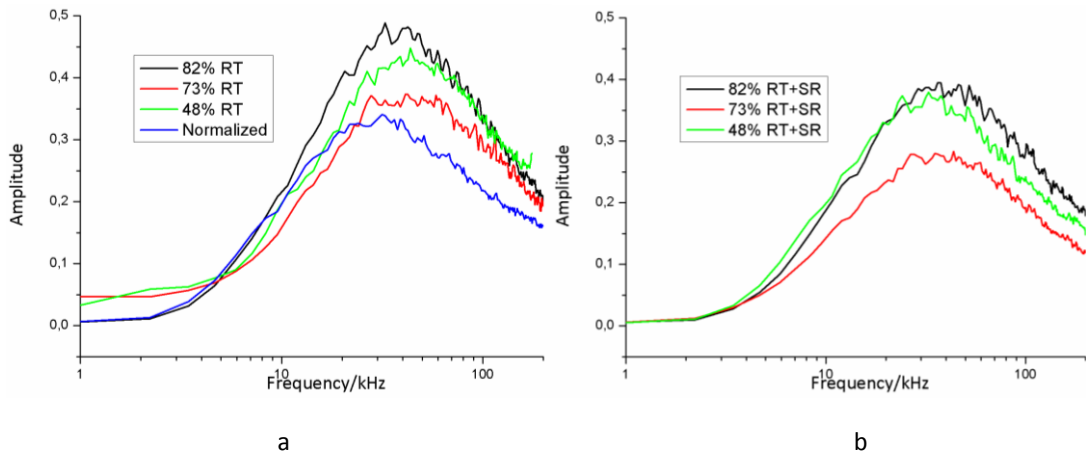
Figure 3-36 MBN frequency spectrums in the transverse direction a) temper rolled (%RT), b) stress relieved (%RT+SR)

3.6.2.3 Hysteresis Curves

Hysteresis curves obtained by μ-scan measurements for the rolling and transverse directions are given in Figure 3-37 and 3-38, respectively. In general, the slopes and the widths of the curves increase with increasing reduction in thickness. Application of stress relief or normalization heat treatment reduces the slope, and also the values of coercivity and retentivity.
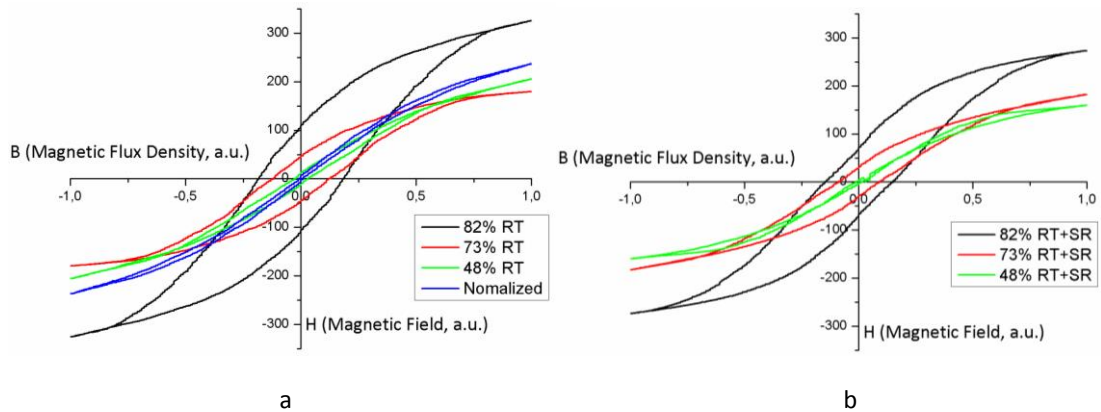
Figure 3-37 Hysteresis curves in the rolling direction a) temper rolled (%RT), b) stress relieved (%RT+SR)
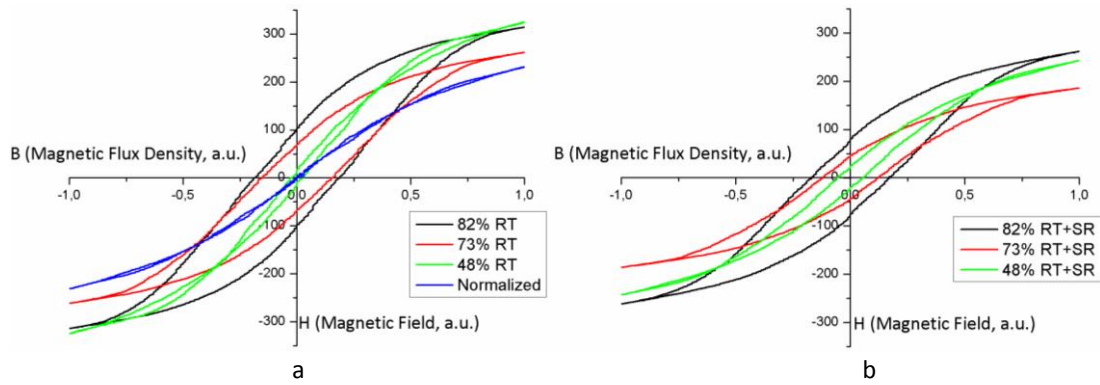
Figure 3-38 Hysteresis curves in the transverse direction a) temper rolled (%RT), b) stress relieved (%RT+SR)

Similar variations in the magnetic anisotropy were observed in the hysteresis curves of the samples. For the temper rolled series, 48% and 73% RT samples have harder magnetic properties in the transverse direction than they have in the rolling direction while 82% RT specimen has isotropic magnetic properties. For the stress relieved series, 48% RT+SR specimen has higher coercivity and retentivity values in the rolling direction, while for 73% and 82% RT + SR samples these values are higher in the transverse direction.

Due to recrystallized state in the normalized sample, magnetically soft behavior in the rolling and transverse directions is observed.

In all sample series, the sheets become magnetically harder due to formation of higher pinning sites after high reductions in thickness. In other words, coercivity, retentivity and magnetic saturation points increase with increasing dislocation density or dislocation tangles in the microstructure.

Chapter 4

CONCLUSION

The aim of this study was to non-destructively investigate the effect of texture on magnetic anisotropy. Two specimen series having different texture conditions and residual stress states were prepared from the unalloyed low-C steel sheets in the temper-rolled condition, namely 48%, 56%, 64%, 73%, 77%, and 82%. The effects of percent reduction in thickness and subsequent stress-relief heat treatment on the material were investigated by microstructural examinations, hardness and tension tests, obtaining pole figures via X-Ray diffraction, and measuring residual stress via X-ray diffraction. Magnetic anisotropy maps were obtained by Magnetic Barkhausen noise measurements with 10º rotation steps on the surfaces of the samples. All results were evaluated and correlated. The following conclusions can be drawn from this particular study.

MBN emission created by domain wall motions is very sensitive to the changes in the microstructure such as variation of average grain size, dislocation density, and residual stress state due to temper rolling and subsequent heat treatments.

The magnetic anisotropy maps of the low-C metal sheets with ferritic microstructure, giving information about the texture condition, can be rapidly and non-destructively obtained by MBN measurements.

Signal peak height, fingerprint, frequency spectrum and hysteresis curve obtained from MBN raw data might be used to detect variations in texture condition of low-C steel sheets. However, obtaining reliable quantitative results need further research.

In future studies it is recommended to clearly differentiate the effects of all individual parameters on MBN activity, for instance by preparing specimen series of cold-rolled, cold-rolled and recrystallization annealed at different temperatures; by determining the depth profile of residual stresses, and by making EBSD analyses of the microstructure.

REFERENCES

[1]   Dieter G. E., "Mechanical Metallurgy," 1988, pp. 526-530.

[2]   Jiles D., Introduction to Magnetism and Magnetic Materials, London: Chapman and Hall, 1991.

[3]   Engler O., Randle V., "Introduction to Texture Analyses," 2010, p. 72.

[4]   Banabic D., "Plastic Behaviour of Sheet Metal," in *Sheet Metal Forming Processes*, 2009, p. 35.

[5]   Hutchinson W.B., Nilsson K.I., Hirsh J., Annealing Textures in Ultra-low Carbon Steels, Indiana, USA: Metallurgy of Vacuum-Degassed Steels Products, p 109-125, 1990.

[6]   Fukuda M., "The Effect of Carbon Content Against r Value-Cold Reductions Relations in Steel Sheets," *J. Iron Steel Inst. Japan,* vol. 53, no. 4, pp. 559-561, 1967.

[7]   Dieter G. E., "Mechanical Metallurgy," 1988, p. 558.

[8]   Dixit U.S., Dixit P.M., "A Study on Residual Stresses in Rolling," *Int. J. Mech. Tools Manufact.,* vol. 37, no. 6, pp. 837-853, 1997.

[9]   Inagaki H., "Fundamental Aspect of Texture Formation in Low Carbon Steel," ISIJ International, vol. 34, p. 313, 1994.

[10] Inagaki H., Suda T., "The Development of Rolling Textures in Low-Carbon Steels," *Texture,* vol. 1, p. 129-140, 1972.

[11] Almojil M. A., "Deformation and Recrystallization in Low Carbon Steels," Manchester Materials Science Centre, PhD. Thesis, 2010.

[12] Kang J.Y., Kim D.I., Lee H.C., "Texture Development in Low Carbon Sheet Steels for Automotive Application," in *Microstructure and Texture in Steels*, 2009, p. 85-101.

[13] Stefanita C-G., Department of Physics, Queen's University, PhD. Thesis, Ontario, 1999.

[14] Davut K., "Characterization Of Steel Microstructures By Magnetic Barkhausen Noise Technique," Metallurgical and Materials Eng. Dept., Middle East Technical University, Ms. Thesis, Ankara, 2006.

[15] Schroeder K., *Critical Reviews of Solid State Science,* vol. 6, pp. 45-47, 1976.

[16] Barkhausen H., *Physics,* no. 29, p. 401, 1919.

[17] Stefanita C.G., "The Many Sides of Magnetism," *Physics and Astronomy,* vol. 117, pp. 19-40, 2008.

[18] "ASM Metals Handbook," *Nondestructive Evaluation and Quality Control,* p. 17, 1997.

[19] Moorthy V., Shaw B.A., Evans J.T., "Evaluation of tempering induced changes in the hardness profile of case-carburised EN36 steel using magnetic Barkhausen noise analysis," *NDT & E*

International, vol. 36, no. 1, pp. 43-49, 2003.

[20] Chikazumi S., "Physics of Magnetism," Wiley, New York, 1964.

[21] Cullity B.D., Introduction to Magnetic Materials, Addison-Wesley, 1972.

[22] Campos M.A., Sánchez C., "Magnetic Barkhausen Measurements to Evaluate Formation of Heterogeneous Plastic Deformation Zones in Carbon Steel," *PANNDT,* 2007.

[23] Becker R., Döring W., Ferromagnetismus, Berlin: Springer Verlag, 1939.

[24] R. D. Callister W.D., "Magnetic Anisotropy," in *Materials Science and Engineering: An Introduction*, 2012, p. W37.

[25] Krause T.W., Spzunar J. A., Birsan M., and Atherton D. L., Correlation of Magnetic Barkhausen Noise with Core Loss in Oriented 3% Si–Fe Steel Laminates, *J. Appl. Phys.,* vol. 79, p. 3156-3168, 1996.

[26] Krause T. W., Clapham L., Pattantyus A., and Atherton D. L., Investigation of the Stress-Dependent Magnetic Easy Axis in Steel Using Magnetic Barkhausen Noise, *J. Appl. Phys.,* vol. 79, p. 4242-4253, 1996.

[27] Krause T.W., Clapham L. and Atherton D.L., Characterization of the Magnetic Easy Axis in Pipeline Steel Using Magnetic Barkhausen Noise, *J. Appl. Phys.,* vol. 75, p. 1380-1386, 1994.

[28] Krause T.W., Mandal K., Hauge C., Weyman P., Sijgers B. and Atherton D.L., Tensor Magnetic Hysteresis Loops for a Ferrite Permanent Magnet Cube, *J. Magnetism & Magnetic Mater.,* vol. 169, p. 199-206, 1997.

[29] Stefanita C-G., Clapham L., Yı J.-K., Atherton D. L., "Analysis of Cold Rolled Steels of Different Reduction Ratio Using the Magnetic Barkhausen Noise Technique," *Journal Of Materials Science,* vol. 36, p. 2795 – 2799, 2001.

[30] Krauss G., Steels: Heat Treatment and Processing Principles, Ohio: ASM International, 1989.

[31] Grange R. A., "Metallurgical Transactions," vol. 2, p. 65-78, 1971.

[32] Gür C. H., "Utilization of Magnetic Barkhausen Noise Technique for Non-destructive Characterization of Steel: Determination of Microstructure and Residual Stress," Metallurgical and Materials Eng. Dept., Middle East Technical University, Ankara, 2011.

[33] Sakamoto H., Okada M., Homma M., Theoretical Analysis of Barkhausen Noise in Carbon Steels,

 "IEEE Transactions on Magnetics," vol. 23, p. 2236-2238, 1987.

[34] Astie B., Deqaque J., Portesiel J., Vergne R., Influence of the dislocation structures on the magnetic and magnetomechanical properties of high-purity iron, *IEEE Transactions on Magnetics,* vol. 17, p. 2929-2931, 1981.

[35] Bükki-Deme A., Szabo I.A., Cserhati C., "Effect Of Anisotropic Microstructure On Magnetic Barkhausen Noise İn Cold Rolled Low Carbon Steel," *Journal of Magnetism and Magnetic Materials,* no. 322, p. 1748–1751, 2010.

[36] Sagar P.S., Kumar R.B., Dobmann G., Bhattacharya D.K., "Magnetic Characterization of Cold Rolled and Aged AISI 304 Stainless Steel," *NDT&E International,* vol. 38, p. 674–681, 2005.

[37] Jiles D., "Journal of Applied Sciences," vol. 21, p. 1186, 1988.

[38] Saquet O.,Chicois J., Vincent A., *Materials Science and Engineering A,* vol. 269, pp. 73-82, 1999.

[39] Kaplan M., "Characterization of Dual Phase Steels by Using Magnetic Barkhausen Noise Analysis," Metallurgical and Materials Eng. Dept., Middle East Technical University, Ms. Thesis, Ankara, 2006.

[40] Boyacıoğlu B., "Microstructural Characterizatıon of Hypoeutectoid Steels Quenched from the Ae1 - Ae3 Intercritical Temperature Range by Magnetic Barkhausen Noise Technique," Metallurgical and Materials Eng. Dept., Middle East Technical University, Ms. Thesis, Ankara, 2006.

[41] Kameda J., Ranjan R., Nondestructive Evaluation of Steels Using Acoustic and Magnetic Barkhausen Signals, Effect of Carbide Precipitation and Hardness, *Acta Metallurgica,* vol. 35, p. 1515-1526, 1987.

[42] Tönshoff H.K., Friemuth T., Oberbeck I., Seegers H., "Micromagnetic Stress Determination on Tailored Blanks," in *15th World Conference on Nondestructive Testing*, Roma, 2000.

[43] Dhar A., Clapham L., Atherton D.L., "Influence of Uniaxial Plastic Deformation on Magnetic Barkhausen Noise in Steel," *NDT&E International,* vol. 34, pp. 507-514, 2001.

[44] Stefanita C-G., Clapham L., Yı J.-K., Atherton D. L., "Plastic versus Elastic Deformation Effects on Magnetic Barkhausen Noise in Steel," *Acta Material,* vol. 48, pp. 3545-3551, 2000.

[45] Franco F. A., Gonzalez M. F. R., Campos M. F., Padovese L. R., "Relation Between Magnetic Barkhausen Noise and Hardness for Jominy Quench Tests in SAE 4140 and 6150 Steels," *Journal of Non-Destructive Evaluation, p. 93-103,* 2012.

[46] Maru M., Padovese L., Pérez-Benıtez J. A., Capó-Sánchez J., "Evaluating Plastic Deformation by the Magnetic Barkhausen Noise," *ECNDT,* 2006.

[47] Vengrinovich V.L., Tsurman V.L., "Stress and Texture Measurement Using Barkhausen Noise and Angular Scanning of Driving Magnetic Field," in *WCNDT*, 2004.

[48] Liu T., Kikuchi H., Kamada Y., Ara K., Kobayashi S., Takahashi S., "Comprehensive Analysis of Barkhausen Noise Properties in the Cold Rolled Mild Steel," *Journal of Magnetism and Magnetic Materials,* no. 310, p. 989–991, 2007.

Table A.1 Roll Scan measurements of the temper rolled and the normalized samples

Angle	#1	#2	#3	#4	#5	#6	Normalized
0°	46,64	49,94	84,4	100,62	107,51	119,98	58,27
10^0	46,74	50,75	82,28	93,6	104,36	116,58	57,74
20^0	49,24	52,6	80,78	86,09	102,27	114,28	55,69
30°	53,97	54,42	78,53	75,53	101,02	115,16	53,26
40°	60,68	64,71	76,82	64,86	100,44	106,21	53,02
50°	69,11	74,68	76,84	57,43	98,74	106,36	51,38
60°	79,5	83,89	76,46	50,76	96,56	105,73	50,75
70°	88,87	91,83	76,18	47,5	96,35	109,67	50,08
80°	91,96	96,23	77,27	44,5	98,74	113,82	49,51
90°	90,36	94,28	77,12	46,53	101,05	115,26	50,2
100°	87,13	88,71	77,34	49,54	99,81	116,45	50,77
110°	78,4	83,48	77,66	55,18	96,82	118,23	52,77
120°	70,4	75,78	77,9	59,93	97,38	118,2	54,21
130°	61,54	68,39	77,4	72,81	93,25	118,05	55,29
140°	55,03	63,7	78,3	76,22	94,14	116,96	58,31
150°	50,78	58,94	79,35	88,4	95,32	113,97	60,87
160°	47,8	55,55	84,35	95,65	101,5	111,07	60,66
170°	46,59	54,16	88,4	102,17	107,9	113,25	61,92
180°	44,91	53,57	91,07	102,36	114,26	115,6	61,81
190°	45,86	53,69	92,09	98,02	114,98	116,29	62,03
200°	47,72	55,74	92,53	95,5	108,55	117,75	62,77
210°	50,68	59,32	91	91,49	105,06	111,01	62,89
220°	56	65,15	89,91	84,04	98,3	108,23	61,36
230°	63,28	75,01	89,57	74,75	97,63	100,56	61,07
240°	71,98	77,65	86,43	64,02	95,99	99,4	58,68
250°	80,1	78,32	84,33	63,18	94,32	107,42	59,87
260°	89,55	82,06	83,29	61,92	96,79	115,03	58,78
270°	101,47	82,78	85,46	64,13	97,26	116,84	55,27
280°	99,8	81,11	84,56	63,75	96,22	118,38	54,39
290°	93,14	76,47	80,48	66,65	91,49	116,62	54,84
300°	83,56	75,29	82,25	71,15	90,6	114,87	54,71
310°	73,43	71,17	79,48	78,26	90,77	112,94	55,16
320°	64,37	64,03	80,05	87,8	93,6	109,35	52,48
330°	56,64	58,31	81,22	94,07	100,18	109,18	52,42
340°	50,87	53,43	83,66	97,09	104,95	114,77	51,47
350°	46,48	50,11	84,63	100,66	107,54	117,05	55,39

Table A.2 Roll Scan measurements of the stress relieved samples

Angle	#1	#2	#3	#4	#5	#6
0°	44,15	54,86	58,01	49,99	66,68	84,63
10⁰	44,42	54,52	57,73	49,94	61,95	82,18
20⁰	45,17	51,38	56,15	49,77	59,88	78,38
30°	47,22	50,97	54,26	48,52	53,86	74,82
40°	50,13	50,87	53,57	46,83	52,58	72,62
50°	53,66	50,69	53,08	47,17	52,13	71,52
60°	55,35	49,44	53,04	46,76	52,03	72,16
70°	55,99	49,55	51,97	48,14	53,62	73,36
80°	56,61	48,28	51,59	49,31	54,06	73,95
90°	56,46	48,95	51,72	49,31	55,29	75,44
100°	54,56	49,37	51,41	49,18	57,19	76,22
110°	53,77	49,77	51,3	46,34	58,91	77,25
120°	52,25	49,33	50,53	46,77	57,66	79,68
130°	49,48	50,68	50,63	48,4	56,24	81,04
140°	48,74	52,67	51,84	49,85	57,47	84,25
150°	46,67	54,17	53,03	50,35	57,79	86,48
160°	44,51	55,06	54,68	50,77	59,36	89,48
170°	43,24	57,48	56,47	52,58	60,99	93,7
180°	41,35	59,79	57,26	53,54	65,8	94,66
190°	42,08	58,46	57,24	50,84	66,34	93,35
200°	42,9	58,83	56,75	49,72	63	92,78
210°	43,6	56,76	56,31	49,57	60,73	87,25
220°	46,68	54,74	55,05	49,1	57,68	83,67
230°	49,26	54,46	54,52	49,19	56,93	82,45
240°	52,06	52,27	54,1	50,07	56,06	80,24
250°	54,22	52,08	54,58	50,43	58,06	79,47
260°	54,34	51,96	53,95	51,23	57,7	78,97
270°	56,92	50,78	52,48	48,47	58	77,94
280°	55,52	50,7	52,33	47,77	57,26	76,79
290°	53,84	51,74	53,66	47,28	56,62	76,89
300°	51,56	52,57	54,07	46,15	58,42	77,24
310°	49,45	52,24	54,44	46,72	59,64	77,95
320°	47,77	50,56	55,42	47,2	60,05	78,74
330°	46,19	52,53	56,49	47,97	61,41	80,38
340°	44,75	55,8	57,95	49,16	63,43	83,4
350°	44,26	56,28	58,43	50,03	66,51	83,53

Table B.1 The results of the hardness measurements

%RT	Hardness Values									
48	91.1	90.2	94.3	92.5	92.8	92.9	92.2	90.0	94.5	90.5
56	96.8	97.1	100.0	95.2	98.0	95.8	98.0	97.5	97.4	97.5
64	90.4	99.1	92.9	91.7	96.3	98.6	96.6	94.8	94.5	95.5
73	101.5	102.0	97.8	97.4	97.1	92.5	92.0	97.2	96.6	97.9
77	95.1	100.8	95.0	99.2	101.1	98.6	93.4	95.2	94.3	94.8
82	99.1	98.6	101.9	102.2	96.7	99.2	92.8	91.5	92.7	96.8